USING OCEAN AMBIENT NOISE CROSS-CORRELATIONS FOR PASSIVE ACOUSTIC TOMOGRAPHY

A Thesis
Presented to
The Academic Faculty

by

Charlotte Leroy

In Partial Fulfillment
of the Requirements for the Degree
Master of Science in the
Woodruff School of Mechanical Engineering

Georgia Institute of Technology
May 2011

USING OCEAN AMBIENT NOISE CROSS-CORRELATIONS FOR PASSIVE ACOUSTIC TOMOGRAPHY

Approved by:

Dr Karim G. Sabra, Advisor
Woodruff School of Mechanical Engineering
Georgia Institute of Technology

Dr Zhigang Peng
Woodruff School of Mechanical Engineering
Georgia Institute of Technology

Dr David Trivett
Woodruff School of Mechanical Engineering
Georgia Institute of Technology

Date Approved: December 10^{th}, 2010

To Anne and Jean-Pierre

ACKNOWLEDGEMENTS

There were many people that have supported me during my studies thus far at the Georgia Institute of Technology, I will be forever grateful for their support. I would like to give thanks to my thesis committee, Dr. Karim G. Sabra, Dr. Zhigang Peng and Dr. David Trivett. I offer my sincerest gratitude to my supervisor, Dr. Karim G. Sabra, who has supported me throughout my thesis with his patience and knowledge whilst allowing me the room to work in my own way. I attribute the level of my Masters degree to his encouragement and effort. Without him, this thesis would not have been completed or written. I would also like to thank the Georgia Institute of Technology community who made my life easier. I am indebted to all the great teachers throughout my education who led me to take an interest in science. My family and friends have been a continuous support system for me throughout my academic career. I would like to thank my parents for pushing me to excel. To them I give the most thanks. A special thanks goes to Thibaut Loysel whose help with LaTeX and many revisions of my thesis were very helpful. He was there from the beginning and his encouragements kept me going through times that were challenging.

TABLE OF CONTENTS

LIST OF TABLES

LIST OF FIGURES

SUMMARY

Recent theoretical and experimental studies have demonstrated that an estimate of the Green's function between two hydrophones can be extracted passively from the cross-correlation of ocean ambient noise recorded at these two points. Monitoring the temporal evolution of these estimated Green's functions can provide a means for noise-based acoustic tomography using a distributed sensor network. Obtaining an unbiased Green's function estimate requires a sufficiently spatially and temporally diffuse ambient noise field. Broadband ambient noise [200Hz-20kHz] was recorded continuously for one day during the SWAMSI09 experiment (in the Gulf of Mexico, near Panama City, FL) using two moored vertical line arrays (VLAs) spanning 7.5m of the 20m water column and separated by 150 m. The feasibility of noise-based acoustic tomography ([300Hz-1kHz]) was assessed in this dynamic coastal environment over the 24 hours. Furthermore, coherent array processing of the computed ocean noise cross-correlations between all pairwise combinations of hydrophones was used to separate acoustic variations between the VLAs caused by genuine environmental fluctuations (such as internal waves) from the apparent variations in the same coherent arrivals caused when the ambient noise field becomes strongly directional, e.g., due to an isolated ship passing in the vicinity of the VLAs.

CHAPTER I

INTRODUCTION

1.1 Background

Active acoustic tomography [32] is an efficient method for monitoring large ocean areas. However, the practical implementation of commonly accepted acoustic tomography techniques [2] requires the use of expensive low-frequency radiators. Other notable drawbacks are the negative impact of noise on marine mammals and potential coastline noise restriction (e.g. California). In order to overcome the difficulties arising from the use of active noise tomography, passive acoustic tomography techniques using ambient noise have been developed [2].

The random nature of noise and scattered fields tends to suggest limited utility as acoustic fields from random sources or scatterers are often considered to be incoherent. However there is coherence between two sensors that receive signals from the same individual source or scatterer. Indeed, an estimate of the time-domain Green's function (TDGF) between two points can be obtained from the cross-correlation of ambient noise recorded at these two points. For instance, assuming 3D free-space propagation and constant sound speed c and uniform spatio-temporal distribution of white noise sources in 3D, the normalized cross-spectral-density $\widehat{C_{1,2}}(\omega)$ at frequency ω between two receivers 1 and 2 separated by a distance r is given by $\widehat{C_{1,2}}(\omega) = [sin(\omega r/c)]/(\omega r/c)$

$$C_{1,2}(t) \;=\; \frac{1}{2\pi}\int_{-\infty}^{\infty} \widehat{C_{1,2}}(\omega) exp(i\omega t) d\omega, \tag{1}$$

which can be simplified as

$$C_{1,2}(t) = \frac{1}{4\pi}\int_{-\infty}^{\infty}\frac{exp[i\omega(t+r/c)]}{i\omega r/c}d\omega - \frac{1}{4\pi}\int_{-\infty}^{\infty}\frac{exp[i\omega(t-r/c)]}{i\omega r/c}d\omega. \quad (2)$$

Consequently, the time derivative of the correlation function is then related to the 3D free space Green's function since:

$$\frac{d}{dt}C_{1,2}(t) = \frac{1}{4\pi r/c}[\delta(t+r/c) - \delta(t-r/c)]. \quad (3)$$

More specifically, the two terms in Eq. (3) correspond to the anti-causal ($t < 0$) and causal ($t > 0$) Green's function.

In the literature, most experimental results have been obtained by using the Noise Correlation Function (NCF) (and not its derivative) as a close estimation of the Green's function. Indeed, performing a time derivative on experimental data is usually avoided because it could be the source of strong undesirable noise. However, the mathematical demonstration above clearly shows that it is the derivative of the ambient Noise Correlation Function that converges towards the Green's function. An element of understanding is provided in Fig. 1, where ambient noise correlation functions $C_{1,2}(t)$ are plotted versus their derivatives for an infinite bandwidth in Fig. 1(a) and a limited bandwidth signal in Fig. 1(b). The two functions look very different in the infinite bandwidth case, mostly because the zero-frequency component creates the plateau of the correlation function. However, this dc component is usually not a problem in real experiments. In the case of a finite bandwidth problem, the two functions resemble each other. Their principal difference is a $\frac{\Pi}{2}$ phase shift that does not affect the overall shape of the waveform but that could be of importance in the case of tomography applications where exact arrival times need to be estimated. However, it is considered a good approximation in order to get rid of undesired noise which can become an experimental issue when performing the time derivative of the correlation function. Therefore the NCF will be used instead of the time-derivative of the NCF.

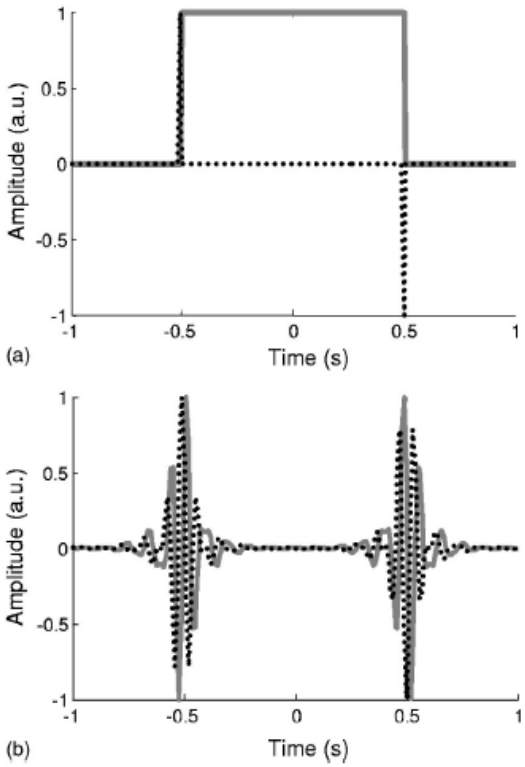

Figure 1: Representation of the noise correlation function (gray line) and its time derivative (black dotted line)(a) in an infinite bandwidth case, with distance=50.25 m and speed=51 m/s; (b) with the same parameters, in a limited bandwidth case [10Hz-20Hz] [Reproduced from Roux et al. [14]]

Recent theoretical and experimental studies in ultrasonics [34], underwater acoustics [19], and seismology [17, 26] have investigated the relationship between the time-domain Green's function (TDGF) and the ambient noise cross-correlation function (NCF) in various environments and frequency ranges. These results provide a means for passive imaging using only the ambient noise field without the use of active sources. The coherent wavefronts emerge from a correlation process that accumulates contributions over time from random sources whose propagation paths pass through both receivers. Figure 2 illustrates the extraction of the TDGF by cross-correlating ambient noise received at sensors located on two different hydrophone arrays located in an ocean waveguide. In the ocean, the dominant seismoacoustic noise source mechanism varies greatly across frequencies from ocean wave generated microseisms (0.05Hz-0.2Hz) to sea-surface noise (above 1kHz), including noise generated by human or biological activities [35].

1.2 Motivation and Goals

Previous theoretical and experimental studies have shown that ocean ambient noise can potentially be used for passive tomography. However, there is still a need to investigate experimentally the asymptotic convergence and emergence rate of the ambient noise cross-correlation function (NCF) towards an estimate of the time-domain Green's function (TDGF) for non-uniform noise source distributions (e.g. shipping noise) in a fast-changing environment. Indeed, correlating ambient noise over a time interval of only a few minutes is typically not enough to be able to extract reliable estimates of the Green's function arrivals with sufficient amplitude (i.e. with high Signal-to-Noise ratio -noted SNR herafter). Longer time intervals of 30 minutes to several hours might be needed depending on the desired SNR. However, the ocean is a fast changing environment and some of the processes we want to be able to monitor (such as internal waves) may evolve over relatively short time scale (tens of minutes).

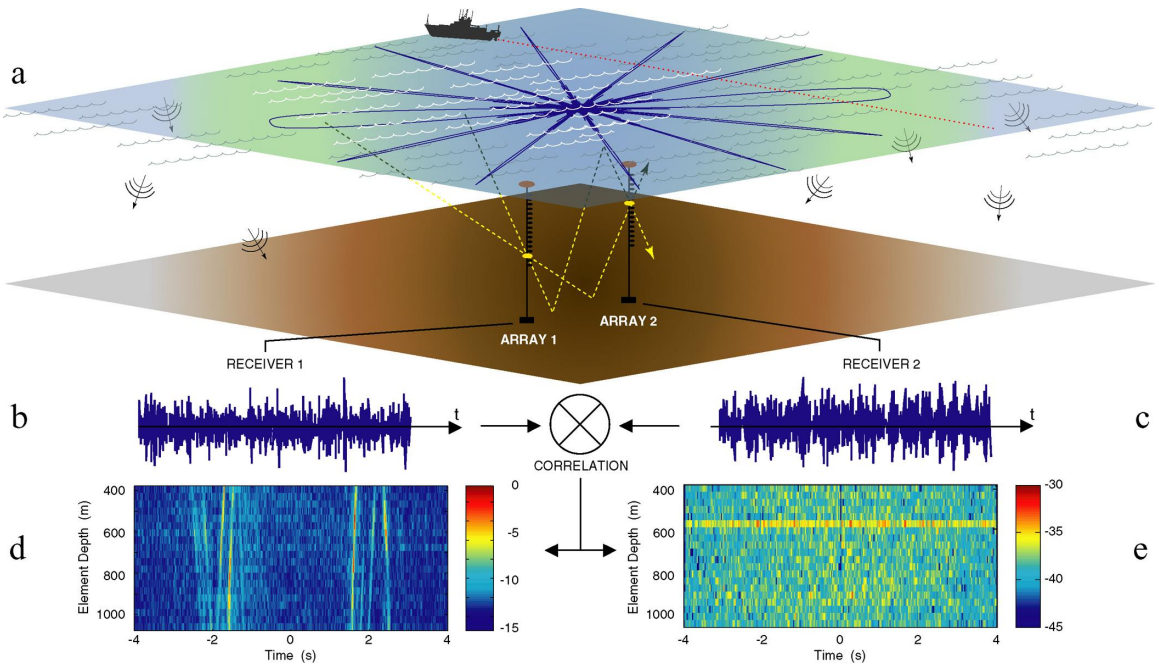

Figure 2: (a) Two arrays are depicted at a separation distance R=2.2 km. A schematic of the directivity pattern of the time-domain correlation process between two receivers on each array is projected on the ocean surface. For the case of equally distributed ambient noise sources, the broad endfire directions will contribute coherently over time to the arrival times associated with the time-domain Green's function (TDGF) while the contribution of the narrow off-axis sidelobes will average down. For the case of shipping noise, coherent wavefronts emerge only when there is sufficient intersection of the shipping paths with the endfire beams. However, if there is a particular loud shipping event, it will dominate so that either impractically long correlation times are needed, or discrete events should be filtered out. (b) and (c) The correlation process is done using time-domain ambient noise simultaneously recorded on two receivers in array 1 and 2. (d) Spatial temporal representation of the wavefronts obtained from the correlation process between a receiver in array 1 at depth 500 m and all receivers in array 2. The arrival structure of the correlation function is composed of the direct path, surface reflected, bottom reflected, etc. as expected in the TDGF. The correlation function is plotted in a dB scale and normalized by its maximum. (e) The same correlation processing is performed on data that have not been recorded at the same time on the two arrays. No coherent wavefront emerge in this case as these two noise recordings are now uncorrelated. [Figure Reproduced from Roux et al, [19]]

Consequently, there is a practical trade off between high SNR and short recording time. The goals of this research are thus to show how different techniques can be used to enhance the emergence rate of coherent wavefronts from ocean ambient noise correlations. These techniques include:

- Time-Frequency preprocessing of ambient noise recordings prior to computing cross-correlations
- Accelerating the convergence rate of the NCF towards the TDGF by using spatio-temporal filtering using receiver arrays

The main focus of this research is on the last point. Different spatio-temporal filtering techniques are used and compared. In particular, in complex environment, the Green's function may not be simply be described by using a ray or modal representation. Spatio-temporal filtering techniques are thus adapted to match the data. In particular, a Singular Value Decomposition is used to produce beamformer weights totally adapted to the data.

1.3 Literature Review

The sources of ocean surface noise (Wenz [35], Andrew [15] and Urick [31]) as well as the subsequent average spatial distribution of ocean noise (Ross [18], Kuperman [11] and Harrison [7]) have been studied extensively.

Experimental and theoretical analyses have shown that the arrival-time structure of the impulse response between a sensor pair can be estimated from the cross-correlation function where, in this case, the noise is ambient vibration. This method was investigated in various environments and frequency ranges. Lobkis [12], Larose [4] and Malcolm [1] focused on ultrasonics. Farrar [5], Caicedo [8], Nagayama [30], Lin [20] and Snieder [29, 16] studied the technique in civil engineering (also referred to as the natural excitation technique [6]). Sabra [23], Shapiro [13] also investigated

this technique for surface wave tomography using ambient seismic noise, and Rickett [17] investigated passive helioseismology (using oscillations at sun's surface recorded optically). More particularly, Roux [19] and Sabra [10, 9] layed the foundations for this research in passive tomography in underwater acoustics.

1.4 Thesis Organization

This section provides the details of how the goals mentioned in section 1.2 are accomplished. Chapter 2 provides a theoretical background which demonstrates how by cross-correlating surface noise (and in particular, shipping noise) it is possible to approximate the Green's function. Chapter 3 presents the experimental setup of the SWAMSI09 experiment. It provides an analysis of the data collected (spectrogram and phase-delay beamforming) and presents the pre-processing steps taken to reduce the influence of high amplitude noise events while preserving the overall phase information of the time series (and thus the arrival-time structure of the noise cross-correlation function). Chapter 4 explains the cross-correlation of ambient noise (CAN) technique and how spatio-temporal filtering and beamforming can be performed to improve the efficiency of CAN. Finally in Chapter 5, the CAN technique is applied to the pre-processed SWAMSI09 ambient noise recordings presented in Chapter 3.

CHAPTER II

THEORY

2.1 Context

Rickett and Claerbout's research in passive helioseismology [17] is based on the following conjecture: "By cross-correlating noise traces recorded at two locations (...), we can construct the wavefield that would be recorded at one location if there was a source at the other." This statement has been theoretically and experimentally confirmed by the seminal paper of Weaver and Lobkis [12], who have shown that the long-time two point correlation of random ultrasonic thermal noise in an aluminum block cavity yields the deterministic time-domain Green's function between the two points. In ocean acoustics, Roux and Kuperman [19] have first demonstrated experimentally that though the sources of ocean noise are uncorrelated, the time-averaged noise correlation function exhibits deterministic waveguide arrival structure embedded in the time-domain Green's function. Their derivation for both volume and surface-noise case is summarized hereafter in section 2.3.

2.2 Green's function

Mathematically, the time-domain Green's functions[1] (TDGF) are the solutions of the wave equations satisfying specific initial or boundary conditions. More specifically in acoustics, it usually refers to the signal received at a certain location when a signal is emitted at another location. While the TDGF function is well known in free space, it can only be modeled approximatively in real cases. For instance in a shallow water waveguide the Green's function becomes more complicated including not only direct

[1] Green's functions are named after the British mathematician George Green who first developed the concept in the 1830s

and reflected path but also attenuation and refraction effects (e.g. see Fig. 2). In a range-independent waveguide, the Green's function is commonly approximated as a simple normal mode expansion at low frequencies ($f < 1kHz$). More specifically, the Fourier transform of the Green's function $G_\omega(R, z_1, z_2)$ at the frequency ω between point 1 at depth z_1 and point 2 at depth z_2 separated by horizontal range R is given by a normal mode expansion:

$$G_\omega(R, z_1, z_2) = \frac{iS(\omega)}{4\rho} \sum_n U_n(z_1) U_n(z_2) H_0^{(1)}(k_n R), \tag{4}$$

where $U_n(z)$ is the depth-dependent and frequency-dependent eigenfunction associated with wave-number k_n, ρ is the density at the source location and $S(\omega)$ is the source spectrum. When integrated over the frequency bandwidth, Eq. (4) becomes the TDGF

$$G_t(R, z_1, z_2) = \int G_w(R, z_1, z_2) \exp(-i\omega t) d\omega \tag{5}$$

The wavefront structure of the Green's function results from modes with similar group speeds constructively interfering over frequency; mathematically the wavefronts can be shown to emerge, for example, from a stationary phase evaluation of Eq. (5) that results from the stationary phase condition $d(k_n R - \omega t) = 0$.

2.3 Cross-correlating ambient noise to approximate the Green's function

This section presents the theoretical basis of the relationship between the NCF and the TDGF in an ocean waveguide when ocean noise is dominated by surface noise sources. For frequencies higher than 1 kHz, ocean noise is dominated by surface noise sources (e.g. white caps). For the lower frequencies [100Hz-1kHz], noise is dominated by shipping traffic (which also act as surface noise sources) or surf noise close to

the continental coastline. Thus, the relative amplitudes of the wavefronts depend on the specific shipping distribution during the recording interval. Shipping noise produces similar results to the surface-noise case but distant shipping emphasizes more horizontally traveling wavefronts than nearby ships for which the wavefronts are more vertical. The subsequent experimental results (see Chapter 5) use data filtered in the [300Hz-1kHz] frequency band where shipping noise is preponderant (over wave or wind generated noise for example).

The following results go more in depth than the overview presented in Section 1.1. In particular, Eq. (6) shows that the correlation function obtained from the hypothetical case of volume ambient noise (i.e. ambient noise sources distributed over all ranges and depths in the waveguide) a good approximation of the Green's function between the two two receivers in a waveguide.

$$C_w(R, z_1, z_2) = \frac{\pi Q^2(\omega)}{4\rho k^2(\omega)} \sum_n U_n(z_1) U_n(z_2) \frac{1}{\alpha_n K_n} [H_0^{(1)}(k_n R) - H_0^{(1)}(-k_n^* R)] \quad (6)$$

The two Hankel functions in Eq. (6) represent two wavefronts traveling between receivers 1 and 2 in opposite directions. Physically speaking, the two wavefronts arise from a uniform volume noise distribution so that at any point, noise is coming from all directions. The modal decomposition written in Eq. (6) is very close to the Green's function decomposition as written in Eq. (4). This means that the correlation function obtained from volume ambient noise recorded at two receivers in a waveguide is a good approximation of the Green's function between the two points.

The derivation can be extended for the surface-noise case (located at the same depth z_s) for which the noise correlation function becomes:

$$C_w(R, z_1, z_2) = \frac{\pi Q^2(\omega)}{4\rho k^2(\omega)} \sum_n U_n(z_1) U_n(z_2) \frac{U_n(z_s)^2}{\alpha_n K_n} [H_0^{(1)}(k_n R) - H_0^{(1)}(-k_n^* R)] \quad (7)$$

The amplitude factor $\frac{U_n(z_s)^2}{\alpha_n K_n}$ in Eq. (7) is the only difference between the volume and surface noise cases. Since this amplitude term will not affect the stationary phase argument that synthesizes the wavefronts, the time-domain surface noise correlation function $C_t(R, z_1, z_2)$ will exhibit the same wavefront structure as the two point Green's function, although the amplitudes of the wavefronts will be shaded by the dipole directionality of the surface noise sources. This means that the correlation function obtained from surface ambient noise is still a good approximation of the arrival structure of the Green's function. This derivation is the theoretical basis for cross-correlating (surface) ocean ambient noise in order to approximate the arrival-time structure Green's function. Roux and Kuperman [19] also show that similar results holds in the case where the noise originates from distributed shipping activity.

2.4 Summary

This chapter shows the theoretical bases behind the postulate that it is possible to correlate ambient noise in order to approximate the Green's function between two spatially separated hydrophones. Ocean noise is typically dominated by surface noise sources. In particular, in the frequency range of interest for this study [300Hz- 1kHz], ocean noise is mostly dominated by shipping noise and surf noise. The derivations borrowed from [19] demonstrate that correlating surface noise recordings enables the emergence of coherent wavefronts from the NCF.

Next Chapter presents the SWAMSI09 experimental set-up and ambient noise data set which will be cross-correlated in Chapter 5.

CHAPTER III

EXPERIMENT

3.1 Experimental Setup

SWAMSI09 experiment was conducted in the bay of Panama City, Florida (see Fig. 3) which is representative of the Gulf of Mexico shoreline. The SWAMSI09 experiment was mainly focusing on object-detection. These data are opportunity data. During its total duration of 2 weeks (March 23 - April 5), bad weather impeded operations during one day. The data presented in Section 3.2 are ambient noise recorded during this day when no active experiment was performed, and research vessels and AUVs were far away from the test site. The sound speed profile was nearly isospeed ($c \approx 1520m/s$) across the whole water depth ($H \approx 20m$). Broadband ambient noise [200Hz-20kHz] was recorded continuously for 24 hours using two moored vertical line arrays (VLAs) spanning 7.5 m of the 20 m water column and separated by approximately 150 m. Table 1 gives the estimated latitude and longitude of arrays VLA1 and VLA2 although the real array localization may vary by a few meters. Figure 4 shows the orientation of the VLAs, VLA1 being the closest to the northward shoreline.

The two VLAs have 16 elements each with 0.5 m interelement spacing (7.5 m aperture) as shown on Figure 5. The sensors are broadband (bandwidth [20Hz 25kHz]) with a sampling rate f_s =50kHz. 1440 recordings, one minute long each, constitute the total 24 hours recording.

ID	Latitude	Longitude
05 VLA1	30 03.245 N	085 43.019 W
09 VLA2	30 03.211 N	085 43.126 W

Table 1: Coordinates of the VLAs

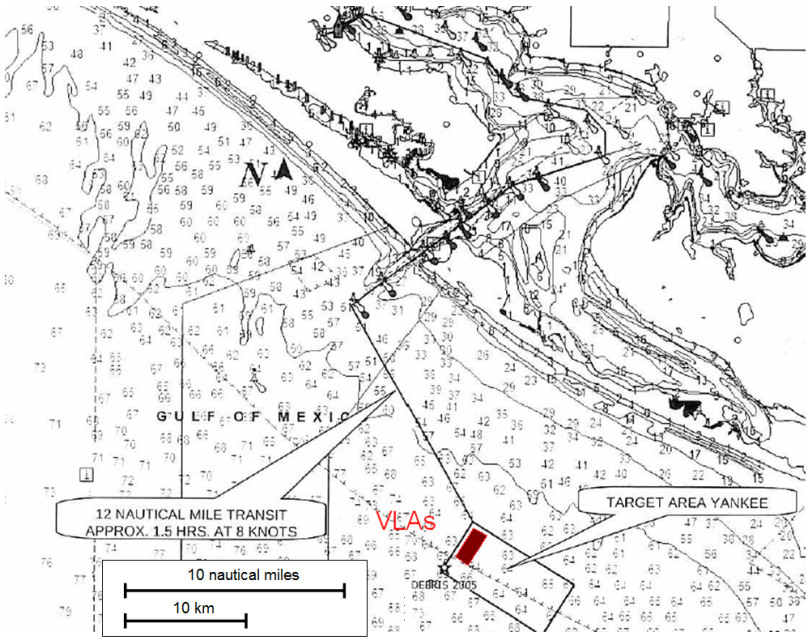

Figure 3: Position of the VLAs area

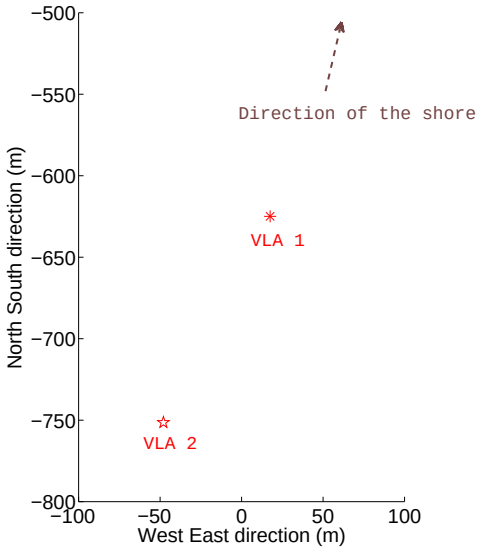

Figure 4: Relative position of the VLAs (metric distance) with respect to an arbitrary origin

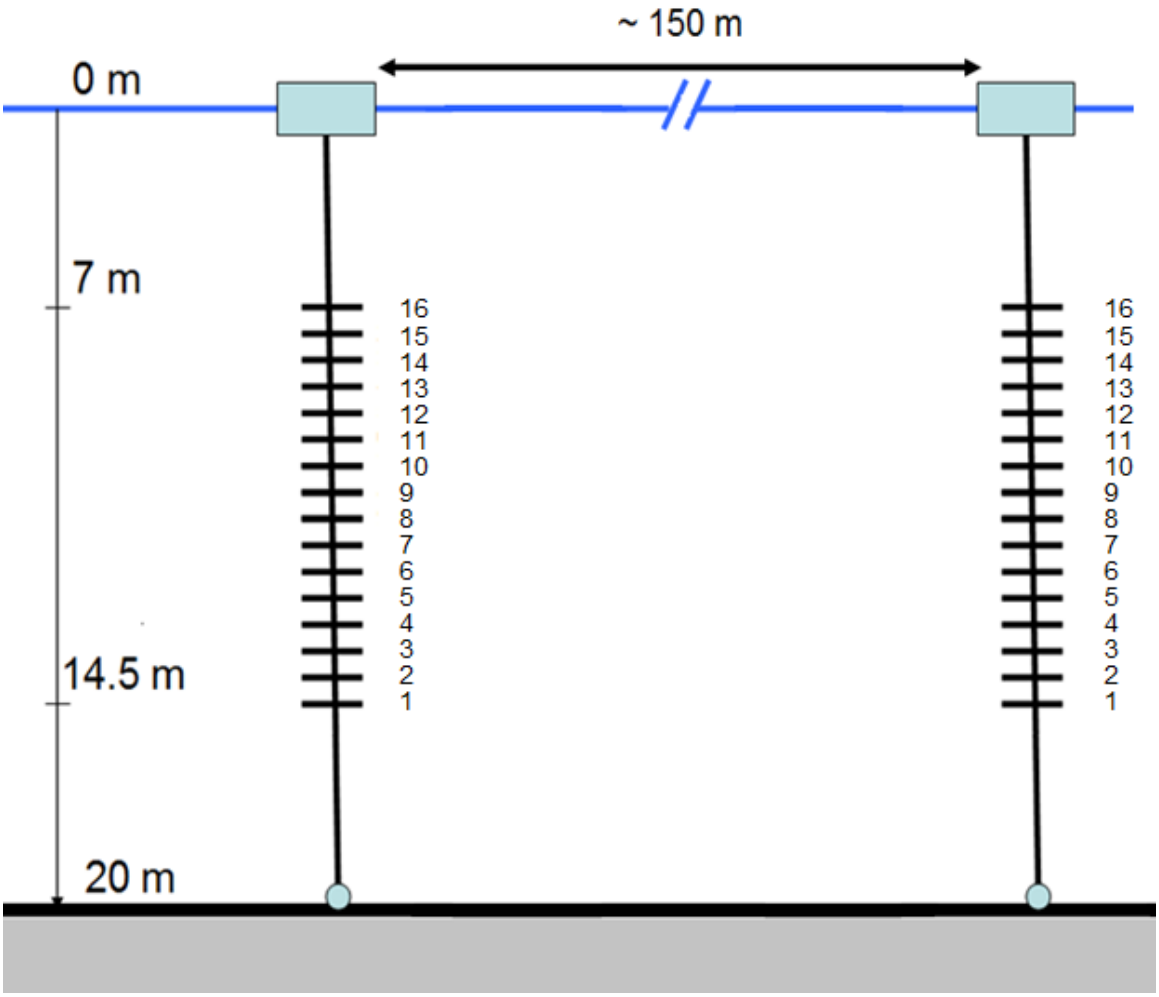

Figure 5: Schematic of the VLA layout in the water column

3.2 Data pre-processing

The SWAMSI09 data can not be used directly. They need to be pre-processed in order to enhance the cross-correlation results as discussed afterwards. In Section 3.2.1, the analysis of the spectrogram of the data for the whole 24 hours is used in order to select the appropriate frequency range where the ambient noise is most energetic. In Section 3.2.2, the vertical angular directionality of the ambient noise field is investigated using a a phase-delay beamformer . Finally, in Section 3.2.3, the findings of the previous sections are used in order to pre-process the data.

3.2.1 Spectrogram

As can be seen on the spectrogram on Fig. 6, ocean ambient noise's magnitude and frequency vary significantly during the experiment. Several observations were considered before selecting the frequency range of [300Hz- 1kHz] to conduct the cross-correlations. First, ambient noise is the loudest in this frequency range. Second, higher frequencies could have been selected as suggested by [19] because it would exclude shipping noise which is more spatially inhomogeneous than wave or wind generated noise. However, as can be seen on Fig. 6, ambient noise levels are low and vary at a fast rate in frequencies $>$ 1kHz where noise is produced by high intensity of wind or waves. Additionally, environmental fluctuations beacome a more serious issue at higher frequencies, which would be detrimental when computing long-time average cross-correlations. These observations lead to the conclusion that the [300 1,000Hz] frequency range where noise is the loudest and varies moderately is likely to be the most appropriate to study the emergence of coherent wavefronts from ambient noise cross-correlations.

3.2.2 Beamforming

A classic phase-delay beamformer was applied to the 24 hours long data set. As can be seen on Fig. 7, ambient noise mostly comes from $[-30^o\ 30^o]$. In shallow water, the

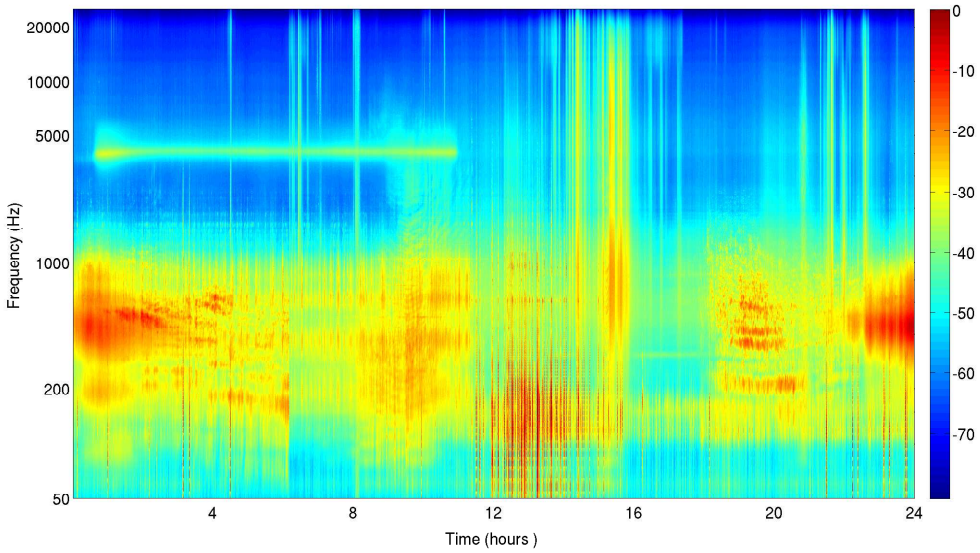

Figure 6: Spectrogram of VLA1 data over a period of 24 hours (dB)

critical angle at the sediment interface (here, sand) limits the propagation of sound along steep paths ($> 30^o$). It also shows that there is no loud close surface-source.

3.2.3 Pre-Processing steps

The recorded ambient noise data over 24 hours were found to be non-stationary with a non-uniform amplitude spectrum as revealed from the spectrogram displayed on Fig. 6. The large amplitude and spectral variations of the recorded ambient noise can bias the coherent arrivals extracted from the noise cross-correlation functions $C_{1,2}(t)$ (see Eq. (8)). The cross-correlation of ambient noise (CAN) technique works best when the background ambient noise field remains fairly stable [10, 25, 9, 23, 33]. Consequently, prior to computing the noise cross-correlation function between all sensor pairs, the noise recordings were pre-processed. Ambient noise data were first filtered in the frequency band [300Hz-1kHz] where the recording amplitude was maximal. The noise field in this band was likely generated by distributed surface noise mainly due to shipping noise and surf noise from the nearby coastline (see Fig. 3). Second, the ambient noise data recorded by each receiver were further

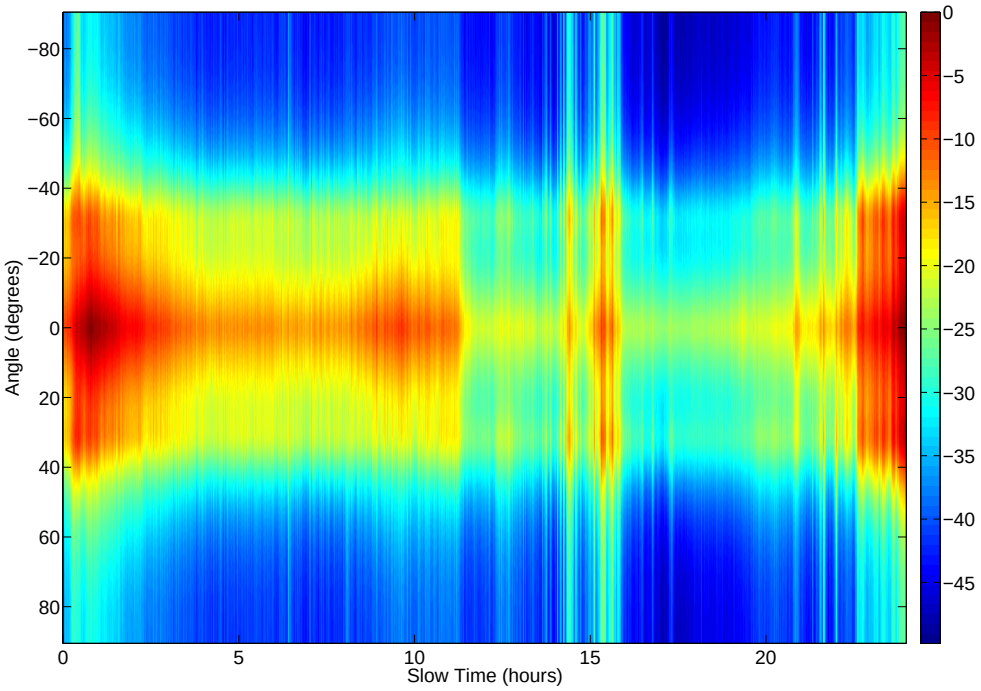

Figure 7: Beamforming of VLA1 data over a period of 24 hours (dB)

homogenized by:

1. Whitening the data spectrum to diminish spectral peaks (e.g. generated by nearby ship's rotating machinery) in order to render the noise spectrum more uniform.

2. Clipping the signal amplitudes to a value of three times the standard deviation computed over all inverse Fourier transform of the frequency-whitened ambient noise data recorded by all receivers.

These two pre-processing steps reduce the influence of high amplitude noise events while preserving the overall phase information of the time series (and thus the arrival-time structure of the noise cross-correlation function) [22]. An exhaustive parametric study (not shown here for the sake of conciseness) was conducted to verify that the selection of both a) the specific smoothing window used for the frequency whitening

operation and b) the specific value of the amplitude threshold for both amplitude clipping operations (by varying it between one to ten standard deviations of the noise time-series) had a minimal influence on the computed cross-correlation waveforms. This observation is likely due to the small level of electronic noise, and hence good quality, of the original acoustic ambient noise recordings. Overall, these data pre-processing steps were found to be robust enough to handle the widely-varying time series recorded during 24 hours at the test site.

3.3 Summary

This chapter presents the experimental setup of the SWAMSI09 experiment and a brief study of the recorded ambient noise. The pre-processing steps are decided after analysis of the data (spectrogram and phase-delay beamforming). The cross-correlation of ambient noise (CAN) technique works best when the background ambient noise remains fairly stable. Consequently, ambient noise data were first filtered in the frequency band [300Hz-1,000Hz] where the recording amplitude was maximal. The ambient noise data recorded by each receiver were further homogenized by whitening the data spectrum and amplitude clipping was used to mute high amplitude events. These pre-processing steps reduce the influence of high amplitude noise events while preserving the overall phase information of the time series (and thus the arrival-time structure of the noise cross-correlation function).

Next Chapter focuses on explaining the CAN technique that will be applied in Chapter 5 to the pre-processed SWAMSI09 ambient noise data set.

CHAPTER IV

SPATIO-TEMPORAL FILTERING

4.1 The CAN technique: definition of the Cross-covariance matrix between spatially separated arrays

A potential application of the CAN technique is the passive (and thus covert) monitoring or tomography of the oceanic environment. Such an application would likely rely on the use of widely separated receiver arrays (or more generally sub-arrays of sensors belonging to a distributed network of receivers) which surround the oceanic region of interest. In this experiment, two distant vertical arrays are used (referred to as VLA1 and VLA2, see Fig. 5) in a set-up typical of an ocean acoustic tomography experiment in shallow water [32]. Note that the methodology developed hereafter can be readily applied to any comparable configuration with two distinct receiver (sub-) arrays of arbitrary geometries (e.g. horizontal or tilted arrays). The CAN technique is implemented here by first computing the time-domain cross-correlation function $C_{i,j}(t)$ between all pairwise combination of the ambient noise signals, $S_i(t)$ and $S_j(t)$, recorded respectively by the i^{th} hydrophones of VLA1 ($i = 1..M$) and the j^{th} hydrophones of VLA2 ($j = 1..N$) (note that the number of elements N and M of both receiver arrays can be different).

$$C_{i,j}(t) = \frac{1}{T_r} \int_{-T_r/2}^{+T_r/2} S_i(\tau)\, S_j(\tau + t) d\tau \tag{8}$$

where the variable T_r corresponds to the total recording duration. Although defined here in terms of a single temporal integration, the noise cross-correlation function can be constructed from an ensemble averaged compilation of the cross-correlation functions computed for recordings of shorter duration. Additionally, the spatial origin of the ambient noise field can be assessed with the CAN results. Based on the ordering

of the signals $S_i(t)$ and $S_j(t)$ in the definition of the cross-correlation function in Eq. (8), coherent arrivals of the waveform $C_{i,j}(t)$ associated with positive time delays t correspond to coherent ambient noise propagating successively from VLA2 to VLA1, i.e. originating in the shoreward direction (see Fig. 8). Conversely, negative time delays t correspond to coherent ambient noise propagating successively from VLA1 to VLA2, i.e. originating from the seaward direction. The Fourier transform of each cross-correlation function $C_{i,j}(t)$ is noted $\widehat{C}_{i,j}(f)$ $(i = 1..M, j = 1..N)$. By definition, the $M \times N$ cross-covariance matrix $\widehat{\underline{\mathrm{C}}}(f)$ of the two arrays VLA1 and VLA2 at the frequency f is composed of all pairwise combinations $\widehat{C}_{i,j}(f)$ $(i = 1..M, j = 1..N$. Note that since the VLA1 and VLA2 are two distinct arrays, the cross-covariance matrix $\widehat{\underline{\mathrm{C}}}(f)$ is in general not square nor Hermitian (i.e. $\widehat{C}_{j,i}(f) \neq (\widehat{C}_{i,j}(f))^*$, where the symbol * denotes a complex conjugate).

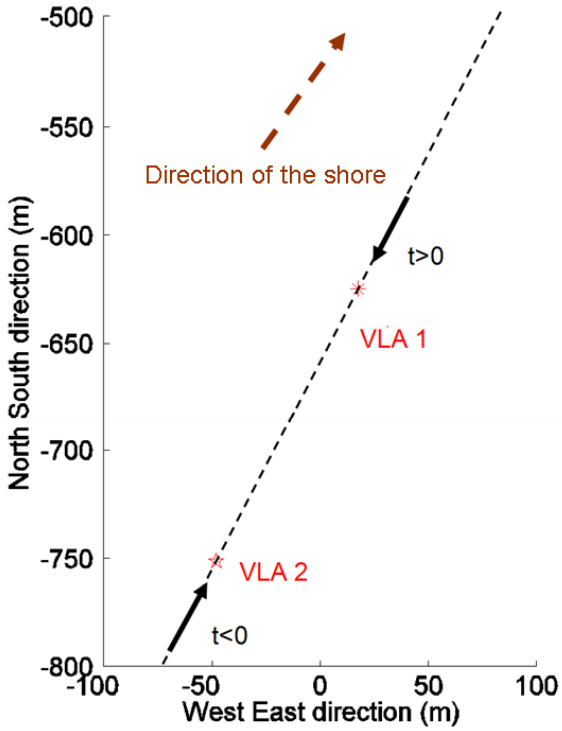

Figure 8: Relative position of the VLAs (metric distance) with respect to an arbitrary origin

4.2 Spatio-temporal filtering of the cross-covariance matrix

4.2.1 Definitions

The original CAN technique relies on extracting the coherent portion of the ambient noise field (i.e. which propagates successively between the two selected receivers) from the incoherent part of the ambient noise field between the selected receiver pairs [19, 10]. However, if receiver arrays are available, standard beamforming technique can thus be readily applied to enhance the spatial directionality of the CAN processing in order to improve the extraction of the coherent portion of the ambient noise field over its incoherent component. Consequently, the use of array beamforming technique can potentially reduce the recording duration T_r (see Eq. (8)) required to extract coherent wavefronts from the ambient noise field between receiver arrays which could have great practical implications in a fluctuating environment. As mentioned in the introductory section, such reduction of T_r is of primary importance when implementing the CAN technique in a fluctuating oceanic environment. For instance, conventional broadband plane wave beamforming (as well as its adaptive variant) has been used to improve the CAN technique for passive imaging of the seabed layers directly below a single receiver array. This passive fathometer processing computes the cross-correlation of the up-looking beam (i.e. selecting the ambient noise propagating from the sea surface) with the down-looking beam (i.e. selecting the ambient noise reflected from the seabed) to extract the coherent portion of the ambient noise field propagating along the vertical array (and thus allowing to estimate the acoustic delays corresponding to the seabed and sub-bottom layers with enhanced precision) [28]. This beamforming approach is generalized hereafter to perform spatio-temporal filtering of the $M \times N$ noise cross-covariance matrix computed between two spatially separated arrays (as introduced in the previous section). The subsequent theoretical derivations will be presented in the Fourier domain where f is the acoustic frequency of interest.

For the case of two spatially separated arrays (or a pair of sub-arrays of sensors),

spatio-temporal filtering of the ambient noise field can be achieved by simply applying different array weight vectors $W_1(f)$ (size $M\times 1$) and $W_2(f)$ (size $N\times 1$) to respectively the $M \times 1$ and $N \times 1$ noise data vectors measured along the two selected receiver arrays (e.g. VLA1 and VLA2, see Fig. 5). More specifically, the spatially filtered version of original $M \times N$ noise cross-covariance matrix at the frequency f, noted $\widehat{\underline{\mathrm{K}}}(f)$, is given by:

$$\widehat{\underline{\mathrm{K}}}(f) = \left(W_1(f)W_1(f)^H\right) \widehat{\underline{\mathrm{C}}}(f) \left(W_2(f)W_2(f)^H\right)^H, \tag{9}$$

where the symbol ^{H} denotes a complex transpose (or Hermitian transform) operation of the selected matrix. By definition, the terms $W_1(f)W_1(f)^H$ and $W_2(f)W_2(f)^H$ correspond respectively to the $M \times M$ and $N \times N$ projection matrices onto the beam-space associated with the array weight vectors $W_1(f)$ and $W_2(f)$. Consequently, the spatially filtered cross-covariance matrix $\widehat{\underline{\mathrm{K}}}(f)$ has the same dimension $M \times N$ as the original cross-covariance matrix $\widehat{\underline{\mathrm{C}}}(f)$; and its entries ($\widehat{K}_{i,j}(f)$ ($i = 1..M, j = 1..N$))are defined in the canonical "array element"-space domain. Otherwise saying, one can reconstruct a spatio-temporal filtered version- noted $K_{i,j}(t)$- of each one of the original cross-correlation waveforms $C_{i,j}(t)$ (computed between the elements i and j of respectively the first and second receiver arrays, see Eq. (8)), from the inverse Fourier transform of the corresponding complex amplitudes $\widehat{K}_{i,j}(f)$. Additionally, if only "'beam-space"' results are desired, the output of the generalized beamformer $\widehat{B(f)}$ associated with the array weight vectors $W_1(f)$ and $W_2(f)$ is directly given by:

$$\widehat{B(f)} = W_1(f)^H \widehat{\underline{\mathrm{C}}}(f) W_2(f), \tag{10}$$

Mathematically speaking, $\widehat{B(f)}$ corresponds to the complex value of the joint projection of the original cross-covariance matrix $\widehat{\underline{\mathrm{C}}}(f)$ along the beam-spaces defined by the vectors $W_1(f)$ and $W_2(f)$ along respectively the first and second receiver arrays.

The corresponding time-domain beamformer output $B(t)$ is simply obtained from the inverse Fourier transform of $\widehat{B(f)}$.

4.2.2 Selection of the array weight vectors

4.2.2.1 Different strategies

In practice, several strategies can be developed for the selection of the array weight vectors $W_1(f)$ and $W_2(f)$ based on the expected curvature of the coherent wavefronts, which typically depend primarily on the frequency band of the ambient noise recordings as well as the local sound-speed profile. On one hand, if the coherent wavefronts extracted between the receiver arrays can be well approximated by propagating plane waves or ray-like arrivals (e.g. typically, $f > 1kHz$ in shallow water), $W_1(f)$ and $W_2(f)$ can be selected according to conventional plane-wave beamformer or turning-point filters delay laws formulation. In this case, the beamformer output formulation $B(t)$ given by Eq. (10) is akin to the double-beamformer formulation presented by [19] between a source and receiver arrays. Additionally, if both arrays VLA1 and VLA2 are identical and the array weight vectors $W_1(f)$ and $W_2(f)$ are selected to be respectively up-looking and down-looking planar beams, the expression of the beamformer output-i.e. $\widehat{B(f)}$ (Eq. (10)) is reduced to the previously published passive fathometer expressions [28]. On the other hand, when recording low-frequency ambient noise in shallow water, the array vectors $W_1(f)$ and $W_2(f)$ can be defined based on the local curvature of the mode shapes or the horizontal wavenumbers of the propagating modes at the receivers locations depending on the geometry of the receiver arrays (e.g. vertical vs. horizontal array) as described in [21] and references therein. These classical strategies for selecting the array weight vectors are referred to as "model-based" approaches, since they require an a-priori model of the acoustic propagation features between the two receiver arrays. Alternatively, if an estimate of the expected values of the cross-covariance matrix $\widehat{\underline{\mathbf{C}}}(f)$ is available as a reference

(which could be obtained from the expected values over long-time recording T_r), empirical (or "data-derived") weight vectors could be defined based on the computed left and right singular vectors of this reference $M \times N$ cross-covariance matrix $\widehat{\underline{\mathbb{C}}}(f)$. Indeed these left and right singular vectors represent physically the pairs of spatial patterns along both receiver arrays (e.g. VLA1 and VLA2) that explains most of the expected spatial structure of the propagating coherent wavefronts between the two receivers arrays. Consequently, those empirical weight vectors would be most suited as spatio-temporal filters to enhance the emergence rate of coherent wavefronts from noise cross-covariance matrix obtained for short recording duration T_r. This alternative strategy is evaluated in the next subsection by using the SWAMSI09 ambient data set to construct suitable empirical weight vectors.

4.2.2.2 Singular Value Decomposition

In order to find suitable empirical weight vectors, the cross-covariance matrix $\widehat{\underline{\mathbb{C}}}(f)$ needs to be decomposed algebraically along both its input and output vector space. In order to do so, the Singular Value Decomposition (SVD) technique is used. The method presentation is derived from [27] and [24]. It states that any matrix X can be written as

$$X = U\Sigma V^T \tag{11}$$

where X is an arbitrary $n \times m$ matrix. $X^T X$ is then a rank r square symmetric $m \times m$ matrix.

- Σ is the diagonal matrix whose entries are the singular values σ_i of X in descending order. $\sigma_i = \sqrt{\lambda_i}$ where the λ_i are the eigenvalues of $X^T X$
- U is the $n \times n$ matrix formed by the orthonormal eigenvectors u_i of $X^T X$ ordered according to the eigenvalues λ_i

- V is the $m \times m$ matrix formed by the orthonormal eigenvectors v_i of XX^T ordered according to the eigenvalues λ_i

One fundamental property is that $Xv_i = \sigma_i u_i$. The SVD method can be seen as a means to decompose a matrix in a set of orthonormal 'input' (u_i) and 'output' (v_i) vectors of decreasing weight (characterized by the σ_i).

A consequence from Eq. (11) is that matrix X can be written as:

$$X = \sum_{i=1}^{r} u_i \sigma_i v_i^T \tag{12}$$

It is then possible to approximate matrix X depending on the relative weights (characterized by σ_i) of the 'input vectors' u_i and the 'output vectors' v_i. Physically, if $\sigma_1 > 0.4 \times (\sum_{i=1}^{16} \sigma_i)$, it means that most of the energy is best described by the first principal component. Thus, u_1 and v_1 provide accurate weight vectors. X can be approximated as $\widetilde{X} \approx u_1 \sigma_1 v_1^T$. It is the first principal component of X. This SVD decomposition will be applied to a reference cross-covariance matrix $\widehat{\underline{\mathrm{C}}}(f)$ (obtained after a long-averaging time T_r) as described in the next chapter.

In this experiment, the SVD method proves very useful. Indeed, the water depth and wavelength are on the same order of magnitude ($L = 20m$ and $\lambda = \frac{v}{f} = \frac{1520}{500} = 3m$) which means that a normal mode expansion could be used to model acoustic propagation. However, as exposed in Chapter 3, the arrays do not span the whole water column. The SVD decomposition of $\widehat{\underline{\mathrm{C}}}(f)$ yields singular vectors which slightly differ from normal mode shapes of the ocean waveguide. Each singular vector is then composed of several modes in this array configuration. The SVD provides empirical weight vectors for the reference cross-covariance matrix $\widehat{\underline{\mathrm{C}}}(f)$ which will be used in Chapter 5 as spatio-temporal filters to enhance the emergence rate of coherent wavefronts from noise cross-covariance matrix during short recording duration T_r.

4.3 Summary

This chapter explains the CAN technique and how spatio-temporal filtering and beamforming can be performed to improve the efficiency of CAN. These techniques involve determining array weight vectors $W_1(f)$ and $W_2(f)$ based on the expected curvature of the coherent wavefronts. If an estimate of the expected values of the cross-covariance matrix $\widehat{\underline{\mathbb{C}}}(f)$ is available as a reference (which can be obtained from the expected values over long-time recording T_r), empirical (or "data-derived") weight vectors can be defined based on the computed left and right singular vectors of this reference cross-covariance matrix $\widehat{\underline{\mathbb{C}}}(f)$. The Singular Value Decomposition method is used to derive the weight array vectors from the reference cross-covariance matrix $\widehat{\underline{\mathbb{C}}}(f)$.

Next Chapter presents the results of the CAN technique on SWAMSI09 data and discusses how spatio-temporal filtering and beamforming can improve the emergence rate of coherent wavefronts from the noise cross-correlation functions NCF computed between two vertical arrays.

CHAPTER V

EXPERIMENTAL RESULTS

This Chapter presents an experimental implementation of the methodology described in Chapter 4, using the data set described in Chapter 3. Section 5.1 presents the pre-processed data: the matrix of cross-correlations for each minute of the 24 hours recorded. It explains how it can be used to build a reference matrix. The reference matrix needs to have the highest possible SNR in order to be an accurate estimate of the Green's function. Its principal components are then decomposed using a SVD as explained in Subsection 4.2.2.2 and used to filter the cross-correlation matrix. This process is done separately for positive coherent arrivals (see Appendix. A for negative coherent arrivals).

5.1 Cross-correlations Matrix

The reference matrix used in order to perform spatio-temporal filtering of the data (as explained in Section 4.2) has a determinant influence on the good correspondence of the spatio-temporal filtering results with the Green's function. The reference matrix will be used as a "filter": the higher its SNR, the better the quality of the filter.

The conventional CAN technique was applied to the ambient noise data in the frequency band [300Hz 1kHz] after these data were first pre-processed as described in Section 3.2. To do so, the 24 hours long ambient noise recording made by each hydrophone were segmented in 1440 consecutive short intervals of duration $T_r = 1$ min each. For each one of these 1440 intervals, the normalized cross-correlations functions $C_{i,j}(t)$ (as defined in Eq. (8)) were then computed between all pairwise combinations of 1-minute long recordings of the i^{th} hydrophone of the first VLA1 ($i = 1..M = 16$) and the j^{th} hydrophone of VLA2 ($j = 1..N = 16$) (see Fig. 5).

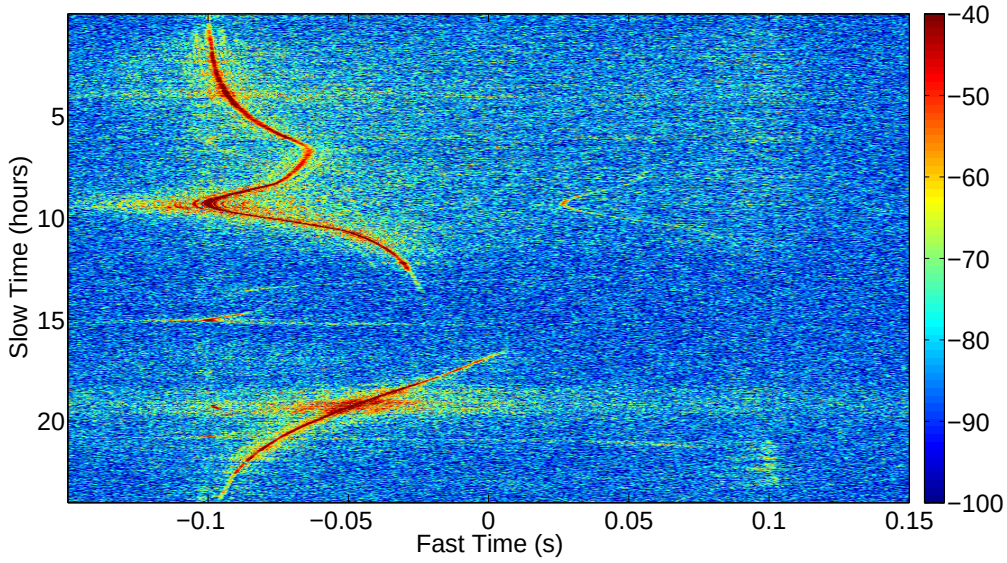

Figure 9: Stacked cross-correlations computed for 1440 1-minute long intervals between element #4 of VLA1 and element #2 of VLA2 (pair (4,2)). Noise data were first pre-processed as described in Chapter 3. The 1440 cross-correlations are stacked along the vertical axis (corresponding to a total duration of 24 hours)

Figure 9 represents the 1440 cross-correlation waveforms, stacked vertically (slow time axis), computed for one representative pair of hydrophone ($i = 4$; $j = 2$). As discussed in Section 4.1, negative time delays t (measured on the horizontal fast time axis) correspond to coherent ambient noise propagating successively from VLA1 to VLA2, i.e. originating from the seaward direction. Fig. 9 shows that the origin, amplitude and generation mechanism of this seaward component of the coherent noise field appears to vary across 24 hours. For instance, the evolution of the isolated high amplitude curve in the negative time delays (e.g. between hours 2 to 10 or hours 16 to 24) most likely results from a loud moving ship whose azimuthal bearing slowly evolves with respect to receiver arrays' location. Indeed, small (resp. large) delays close to $t = 0s$ (resp. $t = -0.1s$) occurs when the ship's location is broadside (resp. endfire) with respect to the vertical plane containing both VLAs [19]. This indicates that the simple time-frequency pre-processing steps (described in the previous section) appears to be insufficient to completely mitigate the effect of isolated coherent loud

sources (i.e. strong interferers) recorded by both receiver arrays. Such loud interferers are problematic as they can create spurious arrivals when computing the long-time average cross-correlation function (i.e. when $T_r = 24$h) by summing all displayed short-time cross-correlations functions $C_{i,j}(t)$ (computed over short duration $T_r = 1$min) for the selected sensor pair (i, j). In particular, previous experimental and theoretical studies [19] have demonstrated that extracting coherent arrival-times of the cross-correlations function $C_{i,j}(t)$ which closely match the arrivals of the actual time-domain Green's function between the selected elements i and j (expected here around $\|t\| = 0.1$s) given the distance between the VLAs (see Fig. 5) require that coherent noise sources should be uniformly distributed within two spatial beams (so called coherent end-fire beams). The endfire beams are aligned on the axis between the two arrays based on stationary phase considerations [29, 19, 10]. The specific angular width (i.e. azimuthal coverage) of those coherent end-fire beams depends primarily on the receiver geometry and the selected frequency content of the ambient noise recordings. Consequently, given the vertical array configurations, the portion of the track of a loud coherent interferer crossing the endfire direction (e.g around hour 10 on Fig. 9) could bias the expected coherent arrival-times structure of the long-time average cross-correlation function $C_{i,j}(t)$ for a significantly long recording duration T_r (e.g. several hours in this case) [34]. Additional processing, beyond the scope of this study, would be required to first remove such loud interferers from the original noise data, in order to subsequently favor the emergence of un-biased coherent arrivals from the long-time average cross-correlation function. On the other hand, Fig. 9 shows that no specific coherent loud interferer signal appears to emanate from the shoreward direction (i.e. coherent ambient noise propagating from VLA2 to VLA1) given the relative uniform amplitude distribution of the 1440 short-time cross-correlation functions over all displayed positive time-delays $0s < t < 0.15s$. Indeed, given the close proximity of shoreline northward from the VLAs locations

(see Fig. 3), no major shipping lane were observed north of the test location during the experiment; and thus no loud ship crossed the coherent end-fire beam northward (i.e. shoreward) of the test site. Thus, the recorded shoreward coherent noise was likely dominated instead by surf noise or potentially diffuse shipping noise reflected from the shoaling coastline. Overall, Fig. 9 indicates that the coherent noise field propagating from the shoreward direction likely results from a more uniform spatio-temporal distribution of noise sources than the seaward component of the coherent noise field.

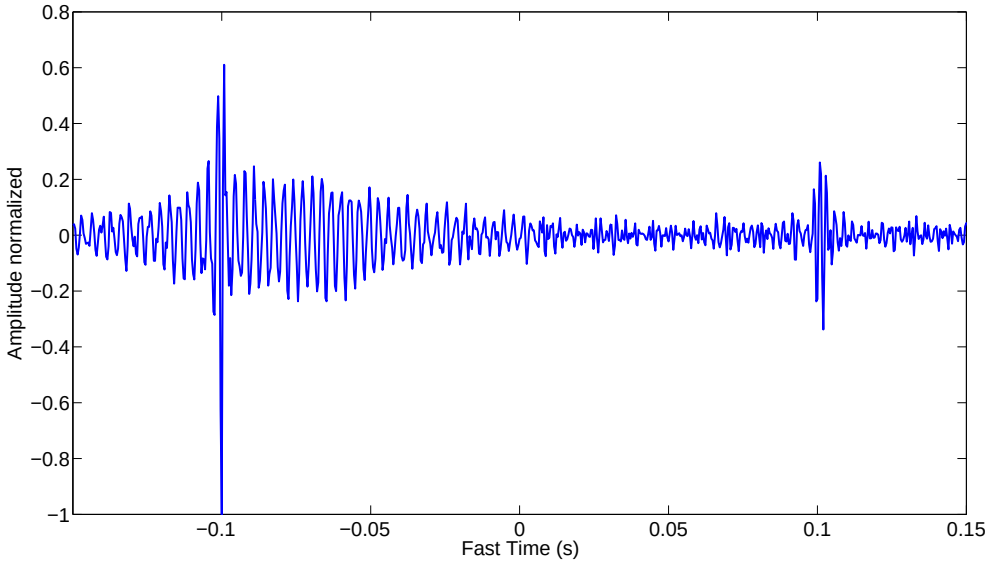

Figure 10: Long-time average cross-correlation wavefront (over 24 hours) between the elements #4 of VLA1 and element #2 of VLA2 used in Fig. 9. This long-time average wavefront was simply obtained by summing all 1440 short-time cross-correlations waveforms shown in Fig. 9 (i.e. summation along the "Slow Time" vertical axis)

Figure 10 displays the arrival-time structure of the long-time average (over 24 hours) cross-correlation functions $C_{i,j}(t)$ between a fixed reference receivers pair $i = 4$ of VLA1 and $j = 2$ of VLA2 for time-delays (same element pair used in Fig. 9). This long-time average wavefront was simply obtained by summing all 1440 short-time cross-correlations waveforms shown in Fig. 9 (i.e. summation along the "Slow

Time" vertical axis). It can be noted that the causal and anti-causal arrival are not perfectly symmetric: their amplitude and shape for $t > 0$ and $t < 0$ are different. As discussed in the previous paragraph, it is hypothesized here that anti-causal coherent wavefronts (i.e. around $t = -0.1$s) are significantly biased by loud interferers (i.e. moving ships here) crossing the endfire beam during some of the 1440 recording intervals (e.g around hour 10 on Fig. 9). Additionally, it was found that the temporal assymmetry of the causal and anti-causal coherent wavefronts could only be slightly reduced by excluding those specific intervals from the summation over 24 hours when computing the long-time average cross-correlation functions (not shown here). Similar results were observed when visualizing the other coherent wavefronts obtained when varying the reference receiver $i = 1..16$ along the aperture of VLA1. Indeed, further signal-processing methodologies would need to be developed to mitigate the spatio-temporal inhomogeneities of the coherent noise sources distribution in the seaward endfire beam. But such developments are beyond the scope of this thesis. On the other hand, as discussed in the previous paragraph, it is hypothesized that the spatial distribution of the coherent noise sources within the shoreward endfire beam is likely to be more homogeneous at this test-site. Consequently, in the remainder of this thesis, the spatio-temporal filtering methodology described in Chapter 4 will only applied-for the sake of conciseness- to the causal coherent wavefronts centered around $t = +0.1$s which are hypothesizes to be less biased. Hence the cross-covariance matrix, introduced in Chapter IV, is formed by computing all pair-wise combinations of the Fourier transform $\widehat{C}_{i,j}(f)$ $(i = 1..16, j = 1..16)$ of the causal portion of the each cross-correlation function $C_{i,j}(t \geq 0)$. The analysis of negative time-delays is done in Appendix. A for comparison.

5.2 Reference Matrix

As explained in Section 4.2, spatio-temporal filtering relies on the use of a reference matrix whose principal components are decomposed using SVD and used to create a "filter" for the cross-correlation matrix $C(t)$. The quality of the reference matrix is primordial in order to be able to use it to reconstruct coherent wavefronts. In this Section, the reference matrix is displayed in order to discuss its quality. First, the wavefront of the reference matrix (constructed by summing the 24 hours) between element #4 of VLA1 and all elements of VLA2 is displayed. Then the cross-correlation matrix with respect to increasing averaging time (from one minute of summation to 24 hours of summation) is displayed in order to discuss the evolution of SNR with respect to averaging time.

5.2.1 Wavefront of the reference matrix

Figure 11(a) shows the wavefront of the reference matrix (constructed by summing the 24 hours) between element #4 of VLA1 and all elements of VLA2. The VLAs are bottom-mounted so there is more tilt at the surface. The signal is louder close to the bottom where VLAs are more stable. The element #4 was chosen because its proximity to the bottom makes it more stable.

The reference matrix was decomposed using SVD (see Eq. (12)) and Fig. 11(b) shows its first principal component $\widetilde{X} = u_1\sigma_1 v_1^T$. As Fig. 11(a) and Fig. 11(b) are very similar, it can be deduced that the first Principal Component is the most influential. Simulations confirmed that $\sigma_1 > 0.4 \times (\sum_{i=1}^{16} \sigma_i)$ across most frequencies. Fig. 12 shows the singular values normalized by the maximum of σ_1. We can draw the conclusion that there is one strong arrival, given the short separation distance between VLAs since all propagating modes arrive at the same time.

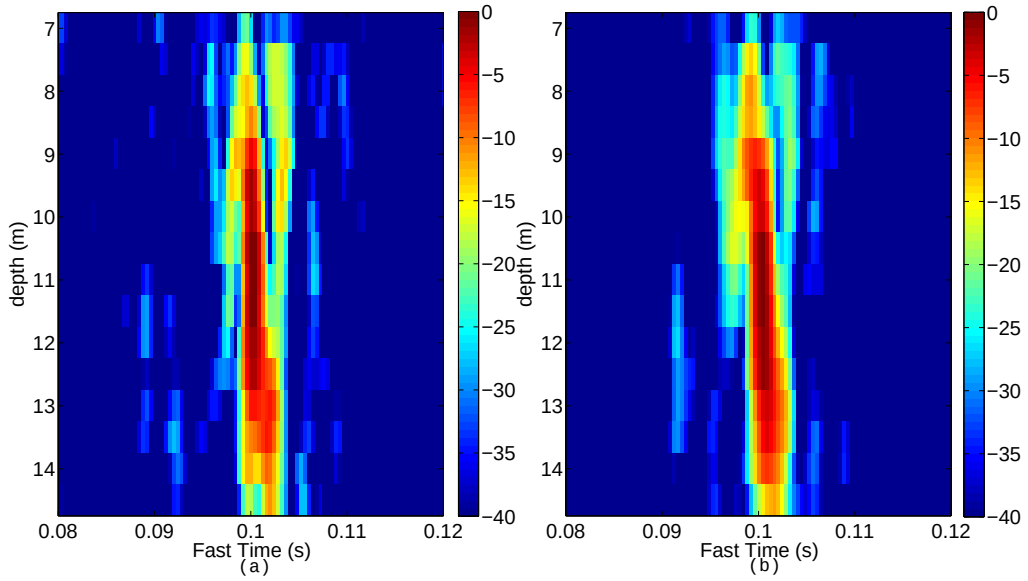

Figure 11: (a) Wavefront (positive arrival) of the selected reference matrix (cross-correlation matrix summed over 24 hours) constructed between element #4 of VLA1 and all elements of VLA2 (b) Broadband reconstruction of the principal component of the cross-covariance matrix $\widehat{\mathbb{C}}(f)$ between the same pair of elements. The first principal component was obtained using SVD (see Eq. (11).

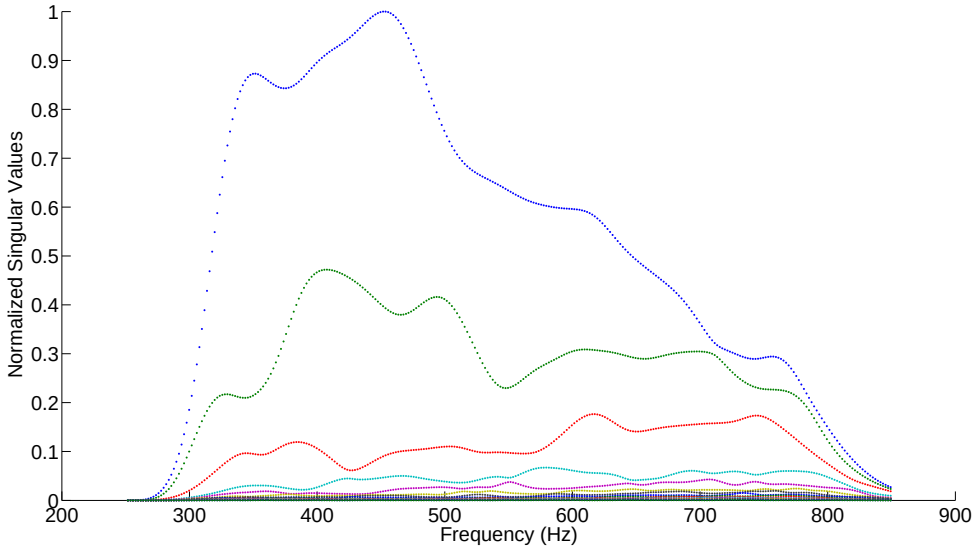

Figure 12: Singular values $\sigma_{i=1..16}$ (see Eq. (12)) of the distribution of the cross-correlation matrix $\widehat{\mathbb{C}}(f)$ across frequencies normalized by the maximum of σ_1. The singular values $\sigma_{i=1..16}$ are sorted by decreasing order.

5.2.2 SNR of the reference matrix

The reference matrix was constructed as the sum over 1440 minutes (24 hours) of cross-correlations. Figure 13(a) displays the cross-correlation matrix with respect to increasing averaging time and Figure 13(b) its SNR. The SNR is computed as follows:

$$SNR = \frac{Signal}{Noise} = \frac{max(Enveloppe(Corr), 0.098 < t < 0.102)}{std(Corr, 0.2 < t < 0.5)} \tag{13}$$

The signal level is estimated as the maximum of the cross-correlation in the time interval where the desired coherent noise peak is. The noise is estimated as the standard deviation of the cross-correlation in a time interval where there is incoherent noise.

The reference matrix constructed by summing 24 hours of cross-correlations has a SNR of 24 dB (see Fig. 13(b)).

5.3 Averaging Time

The SVD decomposition of the reference matrix built in the previous Section is used to filter cross-correlations. In this Section, the filter is applied to the cross-correlation matrices with respect to increasing averaging time in order to discuss the evolution of SNR with respect to averaging time. The goal here is to compare the evolution of the SNR with and without applying filtering and to discuss its efficiency.

5.3.1 Spatio-temporal filtering

Figure 14(a) shows the cross-correlation matrix evolution (for pair (4,2)) with respect to the time of summation of the cross-correlation matrix (from one minute of summation to 24 hours). Figure 14(b) shows the same matrix after spatio-temporal filtering (see Eq. (9)) was applied. The arrival tracking (black crosses) becomes more stable after spatio-temporal-filtering. This is confirmed by Fig. 14(c) which displays the

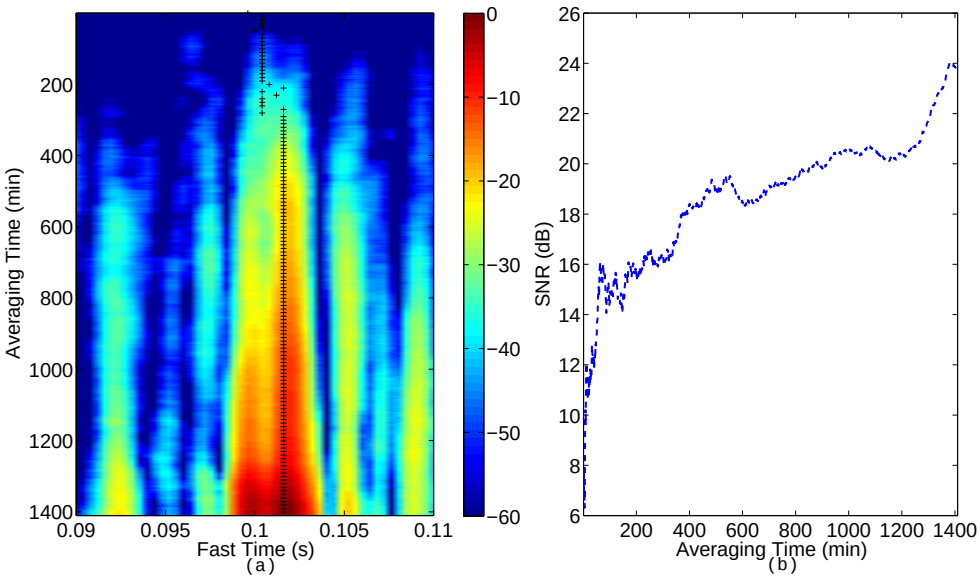

Figure 13: (a) Matrix constructed by summing the cross-correlation matrix (for pair (4,2)) over 24 hours for positive coherent arrivals . The $k-th$ line of the matrix displays the sum of the first k cross-correlations of the 24-hours cross-correlation matrix (which is displayed on Fig. 9) (b) SNR of the matrix displayed left. The value for the $k-th$ minute is the SNR (computed as explained in Eq. (13) of the sum of the first k cross-correlations of the 24-hours cross-correlation matrix

tracked arrival times for the non-filtered and filtered matrices with respect to averaging time. Figure 14(d) shows the evolution of the SNR with respect to the time of summation of the cross-correlation matrix. Figure 14(d) shows that spatio-temporal filtering enables a SNR increase of around 9 dB for the same averaging time T_r.

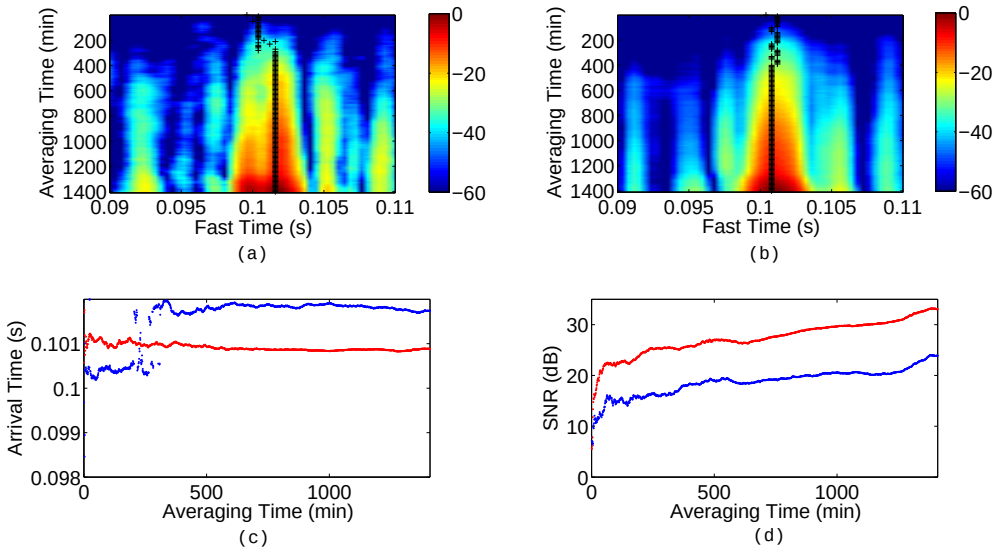

Figure 14: (a) Matrix constructed by summing the cross-correlation matrix (for pair (4,2)) over increasing averaging time for positive coherent arrivals. The $k-th$ line of the matrix displays the sum of the first k cross-correlations of the 24-hours cross-correlation matrix (which is displayed on Fig. 9) (b) Spatio-temporal filtering of the matrix displayed left (c) Coherent Arrival Time before filtering (blue) after spatio-temporal filtering (red) as tracked by the black crosses on the matrices displayed at the top (d) SNR of the matrix displayed at the top left (blue) and top right (red). The value for the $k-th$ minute is the SNR (computed as explained in Eq. (13) of the sum of the first k cross-correlations of the 24-hours cross-correlation matrix (blue) after spatio-temporal filtering (red)

5.3.2 Beamformer output

The beamformer output presented in this section has the same theoretical basis as the spatio-temporal filtering presented in Section 5.3.1. Their difference is the 'output space'. As a reminder of Section 4.2, the spatio-temporal filtering $\widehat{\underline{\underline{K}}}(f)$ of cross-covariance matrix $\widehat{\underline{\underline{C}}}(f)$ is given by:

$$\widehat{\underline{\mathrm{K}}}(f) = \left(W_1(f)W_1(f)^H\right)\widehat{\underline{\mathrm{C}}}(f)\left(W_2(f)W_2(f)^H\right)^H$$

Its beamformer output $\widehat{B(f)}$ is given by:

$$\widehat{B(f)} = W_1(f)^H\widehat{\underline{\mathrm{C}}}(f)W_2(f)$$

Thus, the spatio-temporal filtered matrix $\widehat{\underline{\mathrm{K}}}(f)$ is in the $N \times M$ array's space whereas the beamformer output is in the beam space. Its output is a scalar combining the information of each pair. The beamforming output here produces values around zeros. These are the variations of the arrival time around its mean arrival time (the mean arrival time being the arrival time of the beam as a whole i.e. around 0.1s here). The beamformer output thus differs from spatio-temporal filtering which produces an absolute time arrival.

Figure 15(a) shows the cross-correlation matrix evolution between element #4 of VLA1 and element #2 of VLA2 (pair (4,2)) with respect to the time of summation of the cross-correlation matrix. Figure 15(b) shows the same matrix after beamforming (see Eq. (10)) was applied. The arrival time (black crosses) becomes more stable after beamforming. This is confirmed by Fig. 15(c) which displays the tracked arrival times for the non-filtered and filtered matrices with respect to averaging time. Figure 15(d) shows the evolution of the SNR with respect to the time of summation of the cross-correlation matrix. The SNR for the beamformed matrix is computed as follows:

$$SNR = \frac{max(Enveloppe(Corr), -0.002 < t < +0.002)}{std(Corr, 0.2 < t < 0.5)} \tag{14}$$

Figure 15(d) shows that beamforming enables a SNR increase of around 11 dB for the same averaging time.

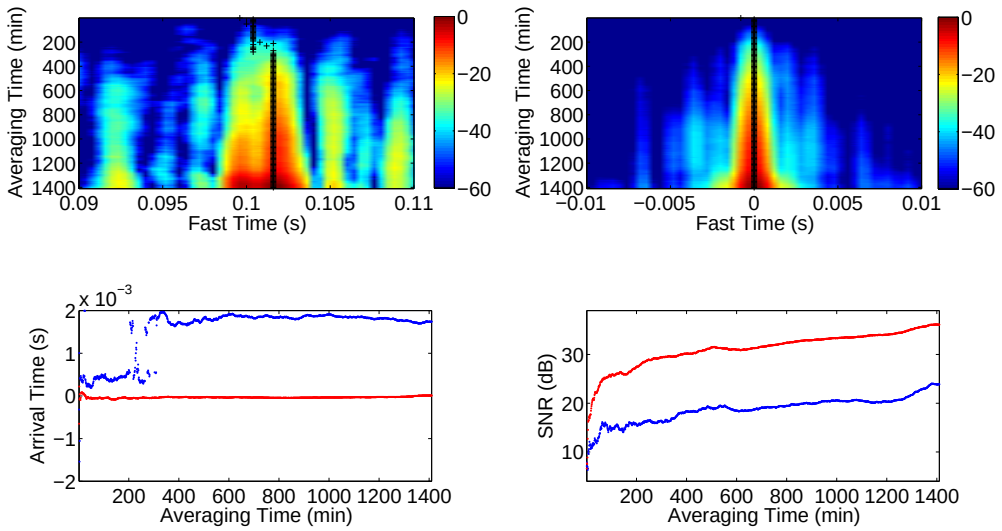

Figure 15: (a) Matrix constructed by summing the cross-correlation matrix (for pair (4,2)) over increasing averaging time for positive coherent arrivals . The $k-th$ line of the matrix displays the sum of the first k cross-correlations of the 24-hours cross-correlation matrix (which is displayed on Fig. 9) (b) Beamforming of the matrix displayed left (c) Coherent Arrival Time (fluctuations around 0.1s) before beamforming (blue) after beamforming (red) as tracked by the black crosses on the matrices displayed at the top (d) SNR of the matrix displayed at the top left (blue) and top right (red). The value for the $k-th$ minute is the SNR (computed as explained in Eq. (13) of the sum of the first k cross-correlations of the 24-hours cross-correlation matrix (blue) after beamforming (red)

5.3.3 SNR for increasing averaging time

A comparison of the evolution of SNR for the non-filtered matrix, the spatio-temporally filtered matrix and the beamformed matrix yields valuable information. Figure 16(a) shows that the beamformed matrix needs only 63 minutes to reach a target SNR of 25 dB. The spatio-temporally-filtered matrix needs 233 minutes. After 24 hours of summation, the non-filtered matrix only reaches 24 dB.

The rate of growth of the SNR for the filtered and beamformed matrices is superior to the rate of growth of the SNR for the non-filtered matrix. This means that these filtering techniques become efficient even for a summation of a few minutes.

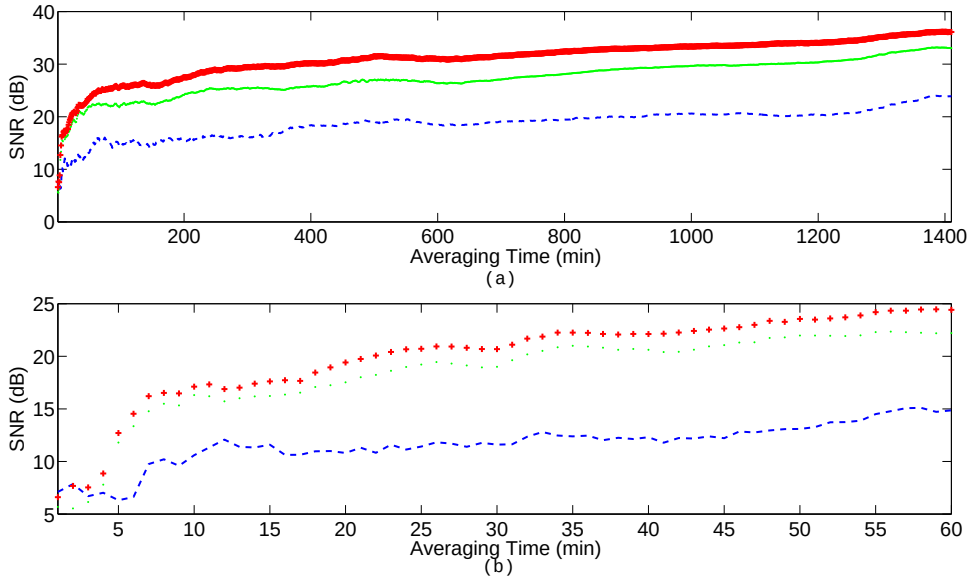

Figure 16: (a) Compared SNRs for positive coherent arrivals before filtering (blue dashes), after spatio-temporal filtering (green dots) and after beamforming (red crosses). The results of Fig. 14(d) and 15(d) were combined (b) Same figure as left but zoomed in on interval [1min 60min]

5.4 Moving Average

In the previous Section, the goal was to compare the length of the summation needed to reach a target SNR depending if the matrix was non-filtered, filtered or beamformed. In this section, the length of the summation is fixed to 30 minutes. This

moving average of 30 minutes is run through the 24 hours of cross-correlation. The variations of the SNR are compared for the non-filtered matrix, the filtered matrix and the beamformed matrix in order to discuss discussing the efficiency of spatio-temporal filtering and beamforming for an averaging time T_r of 30 minutes. The goal is to determine if it is possible to track arrival times with a short summation window of 30 minutes.

5.4.1 Spatio-temporal filtering

When the matrix of cross-correlations is run through a moving average of 30 minutes but non-filtered, it barely allows the wavefront to appear (see Fig. 17(a)). This is confirmed by Fig. 16(b): for 30 minutes of summation the non-filtered matrix has a SNR of only 11 dB. When spatio-temporal filtering is applied to the matrix, the signal appears more clearly as can be observed by comparing Fig. 17(a) and Fig. 17(b). A clearer arrival time in the interval [0.100 0.101s] is observed for the spatio-temporal filtered matrix on Fig. 17(c) compared to scattered points for the non-filtered matrix. The comparison between the SNR of the non-filtered and the filtered matrix (Fig. 17(d)) leads to the conclusion that spatio-temporal filtering enhances the emergence of the wavefront. The SNR of the filtered matrix is superior to the SNR of the non-filtered matrix by 7 dB during most of the experiment. However, the gap between the SNRs vary and for specific times the curves even intersect (e.g. [500 600min]). This finding shows that spatio-temporal filtering does not have the same efficiency during the whole experiment. For example, the [500 600min] time interval is the interval when a boat crosses the endfire beam as mentioned in Section 5.1. Spatio-temporal-filtering does not enhance the reconstruction of the wavefront during this particular time interval. The weight arrays created by SVD are not adapted to the environment created by shipping noise in the endfire beam.

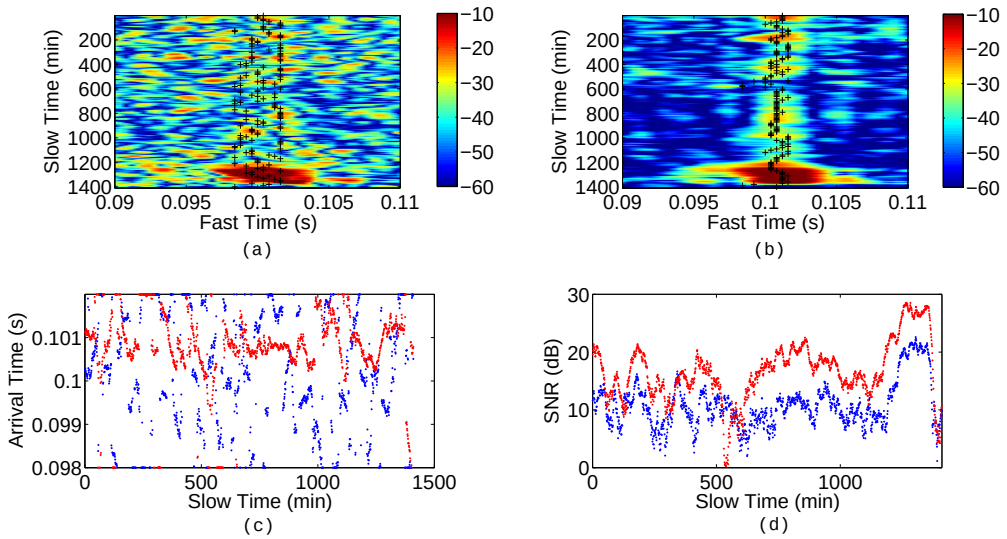

Figure 17: ((a) Matrix constructed by running the cross-correlation matrix (for pair (4,2)) through a moving average of 30 minutes. The $k-th$ line of the matrix displays the sum of the $k-th$ to the $(k+n)-th$ cross-correlations of the 24-hours cross-correlation matrix (which is displayed on Fig. 9) (b) Spatio-temporal filtering of the matrix displayed left (c) Coherent Arrival Time before filtering (blue) after spatio-temporal filtering (red) as tracked by the black crosses on the matrices displayed at the top (d) SNR of the matrix displayed at the top left (blue) and top right (red). The value for the $k-th$ minute is the SNR (computed as explained in Eq. (13) of the sum of the $k-th$ to the $(k+n)-th$ cross-correlations of the 24-hours cross-correlation matrix (blue) after spatio-temporal filtering (red)

5.4.2 Beamformer output

The goal of this Section is to understand how beamforming enhances wavefront reconstruction. Figure 18 compares wavefront reconstruction with or without applying beamforming. When comparing Fig. 18(a) and Fig. 18(b), it is clear that beamforming enhances wavefront reconstruction. It is confirmed by Fig. 18(c) where the beamforming output shows fluctuations around a clear arrival compared to the scattered points of the non-beamformed correlation matrix. The blue points display the variation of the maximum of the correlation for pair (4,2) with respect to 0.1s. Displaying the variations and not the actual value allows a comparison of the arrival time for the non-beamformed and the beamformed matrix even though their output are not in the same space (element space vs beamspace). Fig. 18(d) shows that beamforming enhances the SNR even better.

5.4.3 SNR for a moving average of 30 minutes

Figure 19 displays on the same graph the SNR curves of Fig. 17(d) and Fig. 18(d). Both spatio-temporal-filtering and beamforming enhance the SNR. The SNR increase when using beamforming is higher than when using spatio-temporal filtering. For both techniques, the SNR increase depends on the stability of the environment. When perturbations (such as boats crossing the endfire beam or lull resulting in a significant decrease of ambient noise) occur, there is no SNR increase.

5.5 Summary

In this Chapter, the CAN technique presented in Chapter 4 is implemented on the SWAMSI09 data. The effects of spatio-temporal filtering and beamforming on the emergence of coherent wavefronts from the noise cross-correlation functions (NCF) are then discussed.

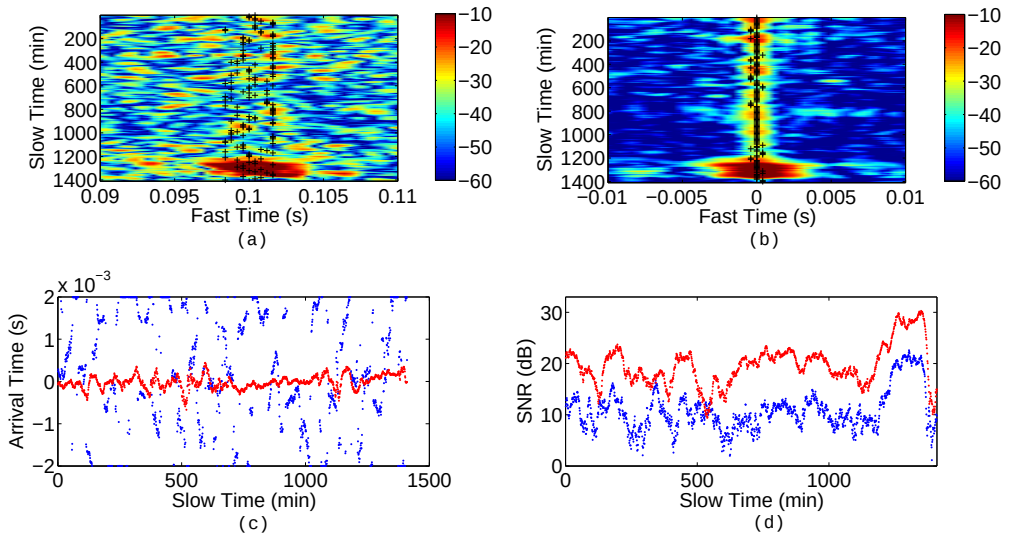

Figure 18: ((a) Matrix constructed by running the cross-correlation matrix (for pair (4,2)) through a moving average of 30 minutes. The $k-th$ line of the matrix displays the sum of the $k-th$ to the $(k+n)-th$ cross-correlations of the 24-hours cross-correlation matrix (which is displayed on Fig. 9) (b) Beamforming of the matrix displayed left (c) Coherent Arrival Time before beamforming (blue) after beamforming (red) as tracked by the black crosses on the matrices displayed at the top (d) SNR of the matrix displayed at the top left (blue) and top right (red). The value for the $k-th$ minute is the SNR (computed as explained in Eq. (13) of the sum of the $k-th$ to the $(k+n)-th$ cross-correlations of the 24-hours cross-correlation matrix (blue) after beamforming (red)

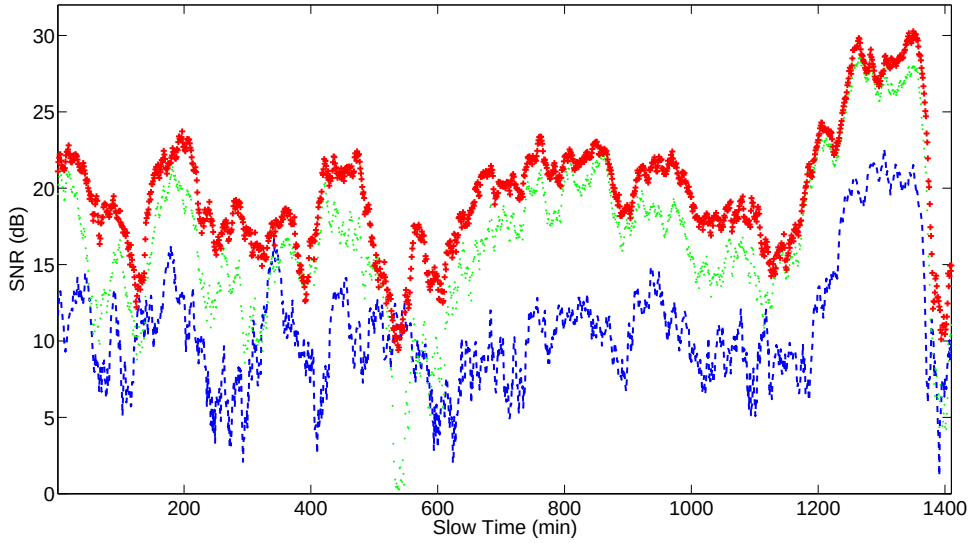

Figure 19: (a) Compared SNRs for positive coherent arrivals before filtering (blue dashes), after spatio-temporal filtering (green dots) and after beamforming (red crosses). The results of Fig. 17(d) and 18(d) were combined (b) Same figure as left but zoomed in on interval [1min 60min]

A reference matrix was built by summing 24 hours of cross-correlations. Its principal components were decomposed using a Singular Value Decomposition and used to filter the cross-correlation matrix. First, the effects of spatio-temporal filtering and beamforming on the cross-correlation matrix with respect to increasing averaging time were discussed. Second, the cross-correlation matrix was run through a moving average of 30 minutes and the effects of spatio-temporal filtering and beamforming were discussed. The method is very efficient for positive time arrivals. It reduces dramatically the number of minutes of summation needed to reach a target SNR. As a result, spatio-temporal filtering and beamforming enables tracking fast-changing fluctuations in the ocean that would not be possible by using only the CAN technique.

The process is less efficient for negative time arrivals (see Appendix. A) because there are more perturbation noise coming from the bay (negative time arrivals) than from the shore (positive time arrivals).

CHAPTER VI

CONCLUSION

Active acoustic tomography is an efficient method for monitoring large ocean areas. However, the practical implementation of commonly accepted acoustic tomography techniques induces notable drawbacks such as the cost of the experiment, the negative impact on marine mammals and potential coastline noise restriction. In order to overcome the difficulties arising from the use of active noise tomography, passive acoustic tomography techniques using ambient noise have been developed. This Thesis investigates experimentally the asymptotic convergence and emergence rate of the time-derivative of the ambient noise cross-correlation function (DNCF) towards an estimate of the time-domain Green's function (TDGF) for non-uniform noise source distributions (e.g. shipping noise) in a fast-changing environment.

During the SWAMSI09 experiment conducted in the bay of Panama City, broadband ambient noise [200Hz 20kHz] was recorded continuously for 24 hours using two moored vertical line arrays (VLAs) spanning 7.5 m of the 20 m water column and separated by approximately 150 m. These data were pre-processed in order to reduce the influence of high amplitude noise events while preserving the overall phase information of the time series (and thus the arrival-time structure of the noise cross-correlation function). After that the CAN technique is implemented on the SWAMSI09 data, the effects of spatio-temporal filtering and beamforming on the convergence of the noise correlation function (NCF) towards the time-domain Green's function (TDGF) are then discussed. First, the effects of spatio-temporal filtering and beamforming on the cross-correlation matrix with respect to increasing averaging time are discussed. Second, the cross-correlation matrix is run through a moving average of 30 minutes and

the effects of spatio-temporal filtering and beamforming are discussed. The method is very efficient for positive time arrivals. It reduces dramatically the number of minutes of summation needed to reach a target SNR. The emergence rate of the estimate of the TDGF is also greatly improved especially in the first tens of minutes. As a result, spatio-temporal filtering and beamforming enables tracking fast-changing fluctuations in the ocean that would not be possible by using only the CAN technique. It is less efficient for negative time arrivals because there are more perturbation noise coming from the bay (negative time arrivals) than from the shore (positive time arrivals).

APPENDIX A

NEGATIVE TIMES

In this appendix, the analysis conducted in Chapter 5 for positive time arrivals is performed for negative time arrivals. All techniques used in this section are the same as those used in Chapter 5.

A.1 Reference Matrix

In order to build the reference matrix for negative time arrivals, analyzing Fig. 9 is useful. It seems logical that there are more perturbation noise coming from the bay (negative time arrivals) than from the shore (positive time arrivals). This hypothesis is confirmed by the presence of bright red signals in the range [-0.1 0s]. These are boats sailing in the bay. There is a risk that their presence might damage the reference matrix only if they approach or cross the endfire beam. Indeed, the reference matrix has a built-in time filter of [-0.11 -0.09s]. Any signal not included in this time interval can not damage the reference matrix. In this section, results with a 24-hour reference matrix are presented. In order to be able to systemize the processes of spatio-temporal filtering it is important to conclude on the results obtained by this method without human intervention needed to select the specific time-interval to build the the reference matrix.

A.1.1 Wavefront of the reference matrix

Fig. 20(a) shows the wavefront of the reference matrix (constructed by summing the 24 hours) between element #4 of VLA1 and all elements of VLA2. Fig. 20(b) shows the same wavefront decomposed on its first principal component using SVD. The first principal component is the most influential.

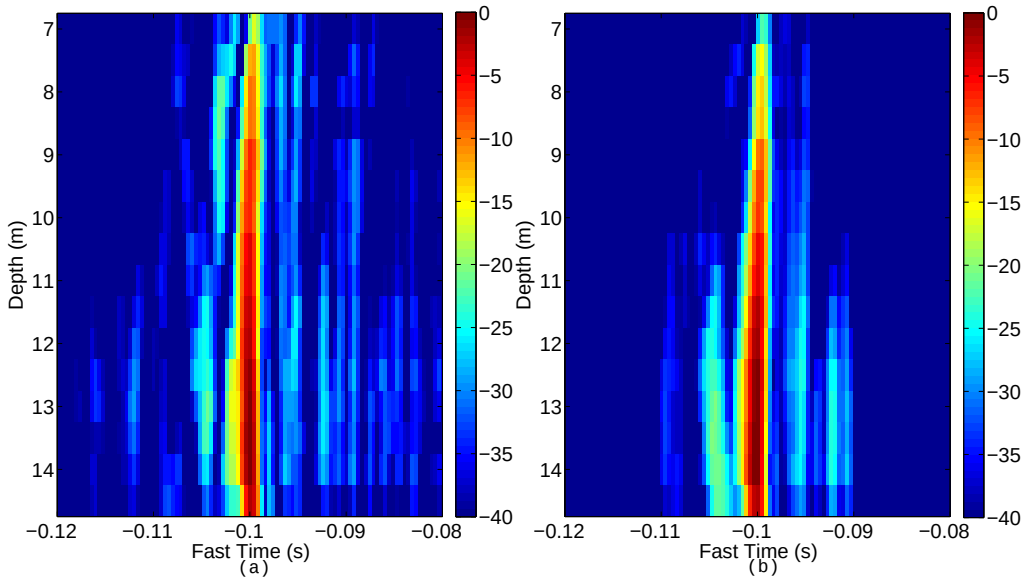

Figure 20: (a) Wavefront (negative arrival) of the selected reference matrix (cross-correlation matrix summed over 24 hours) constructed between element #4 of VLA1 and all elements of VLA2 (b) Broadband reconstruction of the principal component of the cross-covariance matrix $\widehat{\underline{\underline{C}}}(f)$ between the same pair of elements. The first principal component was obtained using SVD (see Eq. (11)

A.1.2 SNR of the reference matrix

The reference matrix was constructed as the sum over 1440 minutes (24 hours) of cross-correlations. Figure 21(a) displays the cross-correlation matrix with respect to increasing averaging time and Figure 21(b) its SNR. The SNR is computed as follows:

The reference matrix constructed by summing 24 hours of cross-correlations has a SNR of 34 dB. However, at time t=551min, the SNR increases sharply. This is due to a boat crossing the endfire beam. The abnormal nature of this event is confirmed by the fact that after the event, the SNR decreases regularly. It can be inferred that even though the boat crossing the endfire beam increases sharply the SNR, this increase is artificial. The weight array vectors extracted by SVD from this reference matrix won't be totally adapted to the environment because they are polluted by a strong artificial signal.

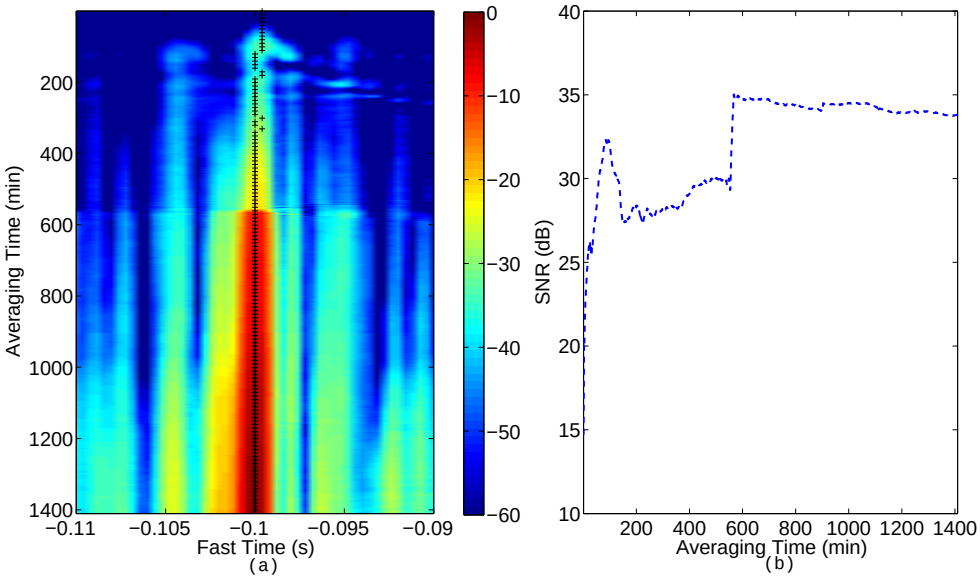

Figure 21: (a) Matrix constructed by summing the cross-correlation matrix (for pair (4,2)) over 24 hours for negative coherent arrivals . The $k-th$ line of the matrix displays the sum of the first k cross-correlations of the 24-hours cross-correlation matrix (which is displayed on Fig. 9) (b) SNR of the matrix displayed left. The value for the $k-th$ minute is the SNR (computed as explained in Eq. (13) of the sum of the first k cross-correlations of the 24-hours cross-correlation matrix

A.2 Averaging Time

The SVD decomposition of the reference matrix built in the previous Section is used to filter cross-correlations. In this Section, the filter is applied the cross-correlation matrices with respect to increasing averaging time in order to discuss the evolution of SNR with respect to averaging time. The goal here is to compare the evolution of the SNR with and without applying filtering and to discuss its efficiency.

A.2.1 Spatio-temporal filtering

Figure 22(a) shows the cross-correlation matrix evolution (for pair (4,2)) with respect to the time of summation of the cross-correlation matrix (from one minute of summation to 24 hours). Figure 22(b) shows the same matrix after spatio-temporal filtering (see Eq. (9)) was applied. Compared to positive times, the arrival tracking (black crosses) is more stable even before spatio-temporal-filtering. This is due to the fact that there is more shipping activity in the bay than in the direction of the shore. This is confirmed by Fig. 22(c) which displays the tracked arrival times for the non-filtered and filtered matrices with respect to averaging time. The arrival time tracked for the non-filtered and the filtered matrices are not exactly the same but they are both quite stable. Figure 22(d) shows the evolution of the SNR with respect to the time of summation of the cross-correlation matrix. Figure 22(d) shows that spatio-temporal filtering enables a SNR increase of around 5 dB.

A.2.2 Beamformer output

Figure 23(a) shows the cross-correlation matrix evolution (for pair (4,2)) with respect to the time of summation of the cross-correlation matrix. Figure 23(b) shows the same matrix after beamforming (see Eq. (10)) was applied. The arrival time (black crosses) becomes more stable after beamforming. This is confirmed by Fig. 23(c) which displays the tracked arrival times for the non-filtered and filtered matrices with respect to averaging time. While the non-filtered matrix tracked arrival decreases

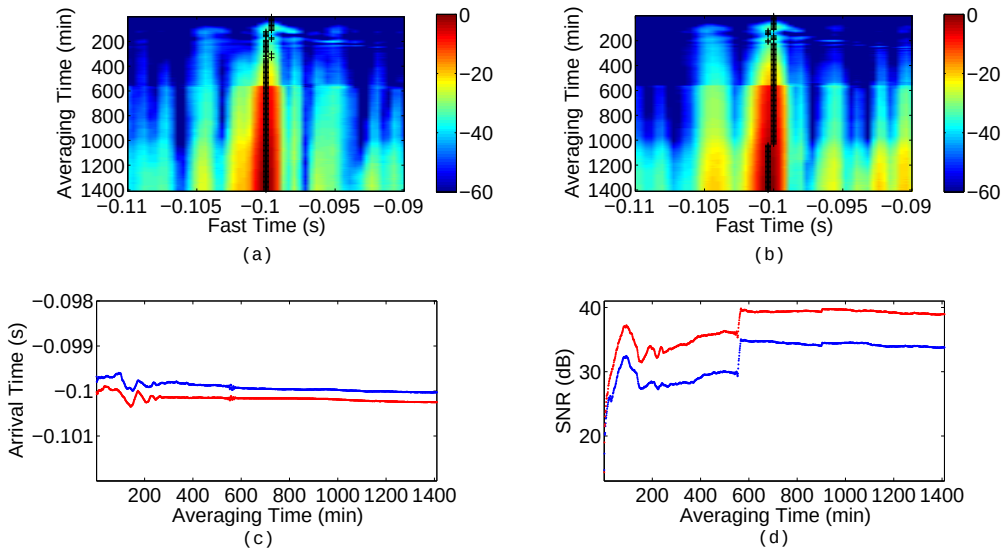

Figure 22: (a) Matrix constructed by summing the cross-correlation matrix (for pair (4,2)) over increasing averaging time for negative coherent arrivals. The $k-th$ line of the matrix displays the sum of the first k cross-correlations of the 24-hours cross-correlation matrix (which is displayed on Fig. 9) (b) Spatio-temporal filtering of the matrix displayed left (c) Coherent Arrival Time before filtering (blue) after spatio-temporal filtering (red) as tracked by the black crosses on the matrices displayed at the top (d) SNR of the matrix displayed at the top left (blue) and top right (red). The value for the $k-th$ minute is the SNR (computed as explained in Eq. (13) of the sum of the first k cross-correlations of the 24-hours cross-correlation matrix (blue) after spatio-temporal filtering (red)

regularly, the beamformed matrix arrival is stable. Figure 23(d) shows the evolution of the SNR with respect to the time of summation of the cross-correlation matrix. The SNR for the beamformed matrix is computed as follows:

$$SNR = \frac{max(Envelope(Corr), -0.002 < t < +0.002)}{std(Corr, -0.5 < t < -0.2)} \tag{15}$$

Figure 23(d) shows that beamforming enables a SNR increase of around 7 dB.

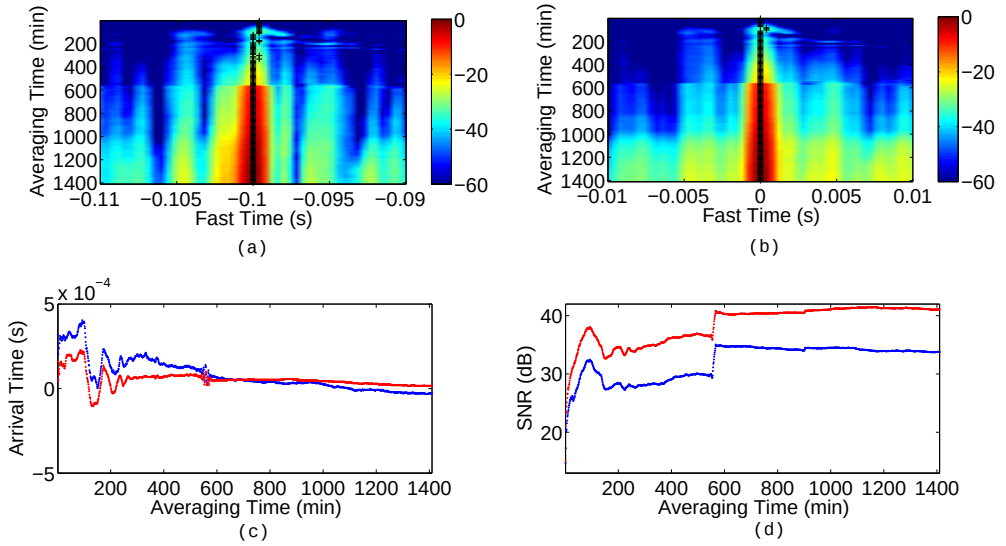

Figure 23: (a) Matrix constructed by summing the cross-correlation matrix (for pair (4,2)) over increasing averaging time for negative coherent arrivals . The $k-th$ line of the matrix displays the sum of the first k cross-correlations of the 24-hours cross-correlation matrix (which is displayed on Fig. 9) (b) Beamforming of the matrix displayed left (c) Coherent Arrival Time (fluctuations around 0.1s) before beamforming (blue) after beamforming (red) as tracked by the black crosses on the matrices displayed at the top (d) SNR of the matrix displayed at the top left (blue) and top right (red). The value for the $k-th$ minute is the SNR (computed as explained in Eq. (13) of the sum of the first k cross-correlations of the 24-hours cross-correlation matrix (blue) after beamforming (red)

A.2.3 SNR for increasing averaging time

The comparison of the evolution of SNR for the non-filtered matrix, the spatio-temporally filtered matrix and the beamformed matrix yields less valuable information for negative arrivals than for positive arrivals. Figure 24(a) shows that the

pollution induced by strong shipping noise (e.g. t=551 min) makes finding a systemic relationship between time of summation and SNR impossible.

The rate of growth of the SNR for the filtered and beamformed matrices is superior to the rate of growth of the SNR for the non-filtered matrix (see Fig. 16(b)). However, the difference is less noticeable than for positive arrivals. The filtering techniques are less efficient for a short time summation.

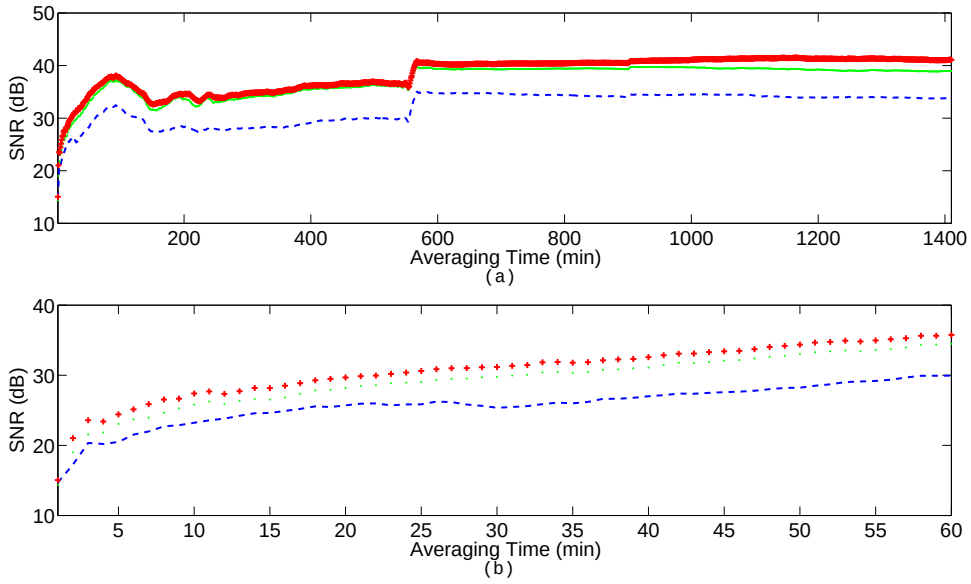

Figure 24: (a) Compared SNRs for negative coherent arrivals before filtering (blue dashes), after spatio-temporal filtering (green dots) and after beamforming (red crosses). The results of Fig. 14(d) and 15(d) were combined (b) Same figure as left but zoomed in on interval [1min 60min]

A.3 Moving Average

A.3.0.1 Spatio-temporal filtering

Fig. 25 compares wavefront reconstruction with or without applying spatio-temporal filtering. Compared to positive arrivals, it appears that the wavefront is already observable on the non-filtered matrix. However, it is enhanced by spatio-temporal filtering as the arrival is clearer (Fig. 25(c)) and the SNR higher (Fig. 25(d)) for the filtered matrix than for the non-filtered matrix.

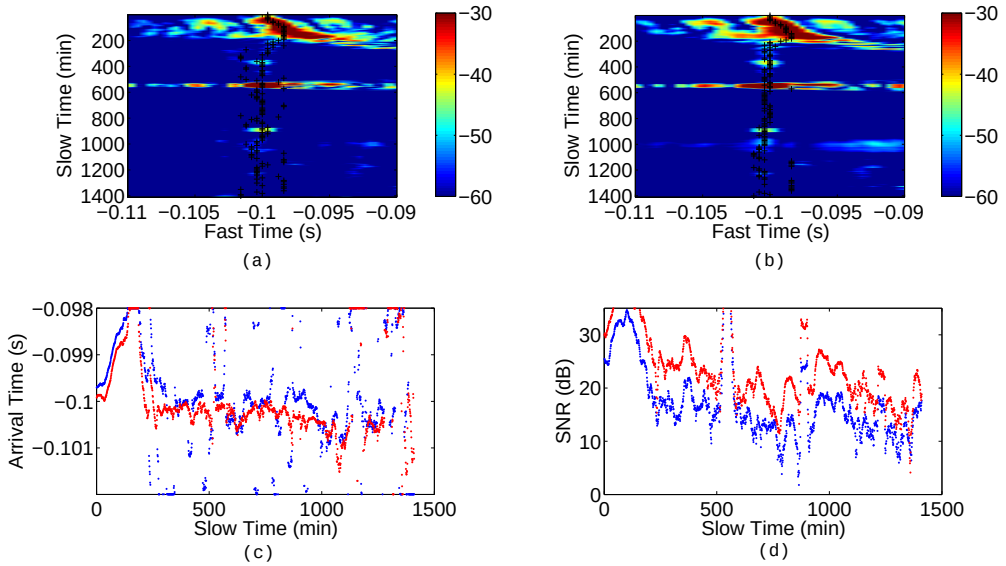

Figure 25: (a) Matrix constructed by running the cross-correlation matrix (for pair (4,2)) through a moving average of 30 minutes. The $k-th$ line of the matrix displays the sum of the $k-th$ to the $(k+n)-th$ cross-correlations of the 24-hours cross-correlation matrix (which is displayed on Fig. 9) (b) Spatio-temporal filtering of the matrix displayed left (c) Coherent Arrival Time before filtering (blue) after spatio-temporal filtering (red) as tracked by the black crosses on the matrices displayed at the top (d) SNR of the matrix displayed at the top left (blue) and top right (red). The value for the $k-th$ minute is the SNR (computed as explained in Eq. (13) of the sum of the $k-th$ to the $(k+n)-th$ cross-correlations of the 24-hours cross-correlation matrix (blue) after spatio-temporal filtering (red)

A.3.1 Beamformer output

Fig. 26 compares wavefront reconstruction with and without applying beamforming. It is enhanced by beamforming as the arrival is clearer (Fig. 26(c)) and the SNR higher (Fig. 26(d)) for the filtered matrix than for the non-filtered matrix.

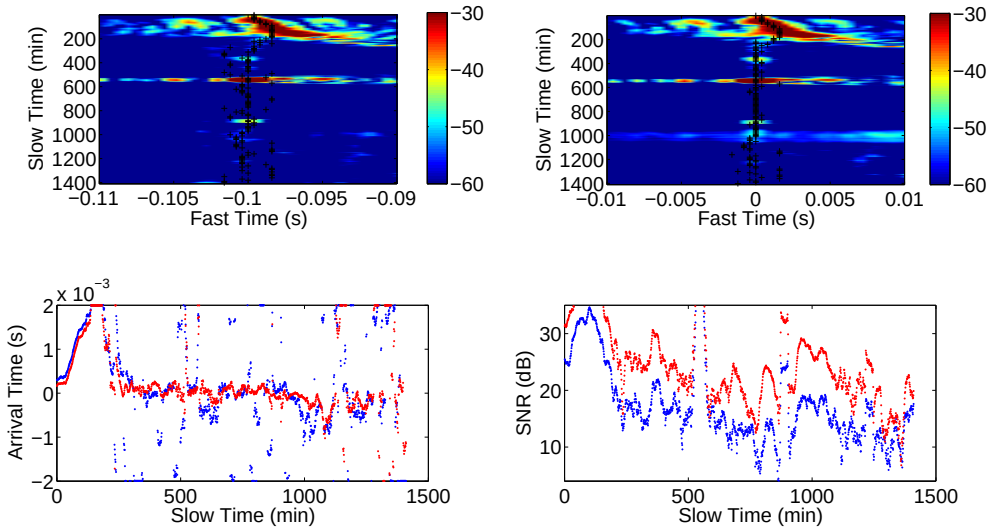

Figure 26: ((a) Matrix constructed by running the cross-correlation matrix (for pair (4,2)) through a moving average of 30 minutes. The $k-th$ line of the matrix displays the sum of the $k-th$ to the $(k+n)-th$ cross-correlations of the 24-hours cross-correlation matrix (which is displayed on Fig. 9) (b) Beamforming of the matrix displayed left (c) Coherent Arrival Time before beamforming (blue) after beamforming (red) as tracked by the black crosses on the matrices displayed at the top (d) SNR of the matrix displayed at the top left (blue) and top right (red). The value for the $k-th$ minute is the SNR (computed as explained in Eq. (13) of the sum of the $k-th$ to the $(k+n)-th$ cross-correlations of the 24-hours cross-correlation matrix (blue) after beamforming (red)

A.3.2 SNR for a moving average of 30 minutes

Fig. 27 displays on the same graph the SNR curves of Fig. 25(d) and Fig. 26(d). Both spatio-temporal-filtering and beamforming enhance the SNR. The SNR increase when using beamforming is higher than when using spatio-temporal filtering. For both techniques, the SNR increase depends on the stability of the environment. The

main perturbation produced by the boat crossing the endfire beam at t=551min is observable. For positive times, it produces an increase in the SNR whereas for negative times a decrease was observable. The increase is due to the fact that when a boat crosses the endfire beam, the noise is magnified.

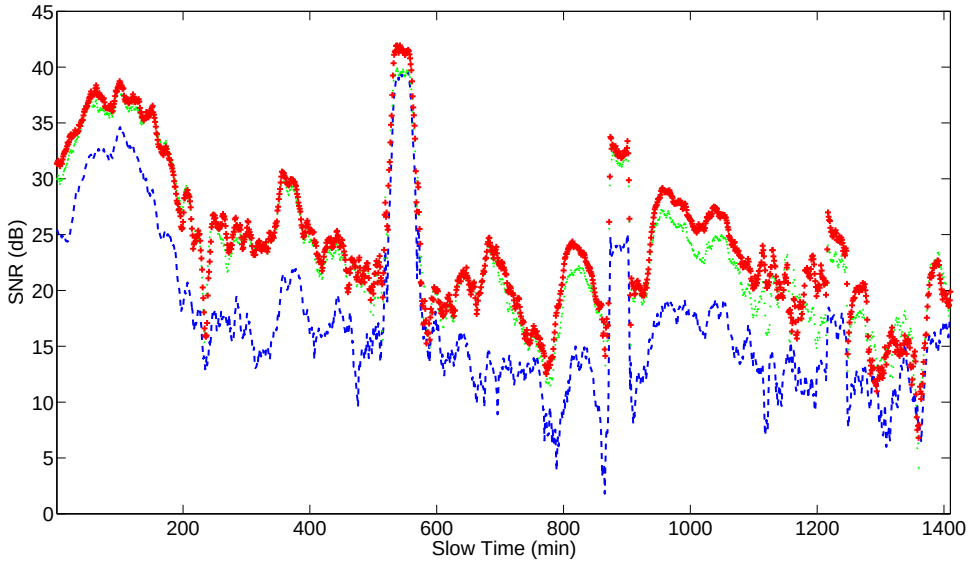

Figure 27: (a) Compared SNRs for negative coherent arrivals before filtering (blue dashes), after spatio-temporal filtering (green dots) and after beamforming (red crosses). The results of Fig. 17(d) and 18(d) were combined (b) Same figure as left but zoomed in on interval [1min 60min]

REFERENCES

[1] A. E. Malcolm, J. A. S. and van der Tiggelen, B., "Retrieving the green function from diffuse equipartitioned waves," *Physical Review Letter*, vol. 70, no. 015601(R), 2001.

[2] Burov, V., Sergeev, S., and Shurup, A., "The use of low-frequency noise in passive tomography of the ocean," *Acoustical Physics*, vol. 54, pp. 42–51, 2008.

[3] Cox, H., "Spatial correlation in arbitrary noise fields with application to ambient sea noise," *The Journal of the Acoustical Society of America*, vol. 54, pp. 1289–1301, 1973.

[4] E. Larose, A. Derode, M. C. and Fink, M., "Imaging from one-bit correlations of wideband diffuse wavefields," *J. Appl. Phys.*, vol. 95, pp. 8393–8399, 2004.

[5] Farrar, C. and James, G., "System identification from ambient vibration measurements on a bridge," *J. Sound Vib.*, vol. 205, pp. 1–18, 1997.

[6] G. James, T. C. and Lauffer, J. P., "The natural excitation technique for modal parameter extraction from operating wind turbines,"

[7] Harrison, C. H. and Simonso, D. G., "Geoacoustic inversion of ambient noise: A simple method," *J. Acoust. Soc. Am.*, vol. 112, pp. 1377–1389, 1980.

[8] J. M. Caicedo, E. Clayton, S. J. D. and Abe, M., "Structural health monitoring for large structure using ambient vibrations," *in Proceeding of the ICANCEER conference, Hong Kong*, pp. 379–384, 2002.

[9] K. G. Sabra, P. Roux, A. M. T. G. L. D. W. S. H. and Kuperman, W. A., "Using ocean ambient noise for array self-localization and self-synchronization," *IEEE J. Ocean Eng.*, vol. 30, pp. 338–347, 2005.

[10] K. G. Sabra, P. R. and Kuperman, W. A., "Arrival-time structure of the time-averaged ambient noise cross-correlation function in an oceanic waveguide," *J. Acoustic. Soc. am*, vol. 117, pp. 164–174, 2005.

[11] Kuperman, W. A. and Ingenito, F., "Spatial correlation of surface generated noise in a stratified ocean," *J. Acoust. Soc. Am.*, vol. 67, pp. 1988–1996, 1980.

[12] Lobkis, O. I. and Weaver, R. L., "On the emergence of the green's function in the correlations of a diffuse field," *The Journal of the Acoustical Society of America*, vol. 110, no. 6, pp. 3011–3017, 2001.

[13] N. M. Shapiro, M. Campillo, L. S. and Ritzwoller, ., "High-resolution surface-wave tomography from ambient seismic noise," *Science*, vol. 29, pp. 1615–1617, 2005.

[14] P. Roux, K. S. and Kuperman, W. A., "Ambient noise cross-correlation in free-space: theoretical approach," *J. Acoust. Soc. Am.*, vol. 117, pp. 79–84, 2005.

[15] R. K. Andrew, B. M. Howe, J. M. M., "Ocean ambient sound: comparing the 1960s with the 1990sfor a receiver off the california coast," *Acoustic Res. Letters Online*, vol. 3, pp. 65–70, 2002.

[16] R. Snieder, J. S. and Calvert, R., "Equivalence of the virtual source method and wavefield deconvolution in seismic interferometry," *Phys. Rev. E*, vol. 73, no. 066620, 2006.

[17] Rickett, J. and Claerbout, J., "Acoustic daylight imaging via spectral factorization: Helioseismology and reservoir monitoring," *The Leading Edge*, vol. 18, no. 8, pp. 957–960, 1999.

[18] Ross, D., "Mechanics of underwater noise," 1987.

[19] Roux, P. and Group, W. A. K. N., "Extracting coherent wave fronts from acoustic ambient noise in the ocean," *The Journal of the Acoustical Society of America*, vol. 116, no. 4, pp. 1995–2003, 2004.

[20] S. Lin, J. Y. and Zhou, L., "Damage identification of a benchmark building for structural health monitoring," *Smart Mater. Struct.*, vol. 14, pp. 162–169, 2005.

[21] Sabra, K., "Blind deconvolution in ocean waveguides using artificial time reversal," *J. Acoust. Soc. Am.*, vol. 116, pp. 262–271, 2004.

[22] Sabra, K., "Emergence rate of the time-domain green's function from the ambient noise cross-correlation function," *J. Acoust. Soc. Am.*, vol. 118, pp. 3524–3531, 2005.

[23] Sabra, K., "Surface wave tomography using microseisms in southern california," *Geophys. Res. Letter*, vol. 32, no. L023155, 2005.

[24] Santamarina, J. C. and Fratta, D., *Discrete Signals and Inverse Problems*. Wiley, 2005.

[25] S.E. Fried, W.A. Kuperman, K. G. S. P. R., "Extracting the local greens function on a horizontal array from ambient ocean noise," *J. Acoust. Soc. Am.*, vol. 124, pp. 8393–8399, 2008.

[26] Shapiro, N. M. and Campillo, M., "Emergence of broadband rayleigh waves form correlations of the ambient seismic noise," *Geophysical Research Letters*, vol. 31, no. L07614, 2004.

[27] Shlens, J., "A tutorial on principal component analysis," 2009.

[28] Siderius, M., "Adaptive passive fathometer processing," *J. Acoust. Soc. Am.*, vol. 127, pp. 2193–2200, 2010.

[29] Snieder, R. and Safak, E., "Extracting the building response using seismic interferometry; theory and application to the millikan library in pasadena, california," *Bull. Seismol. Soc. Am.*, vol. 96, pp. 586–598, 2006.

[30] T. Nagayama, M. Abe, Y. F. and Ikeda, K., "Structural identification of a non-proportionally damped system and its application to a full scale suspension bridge," *J Struct. Eng.*, vol. 131, no. 1536-154, 2005.

[31] Urick, R. J., "Ambient noise in hte sea," 1986.

[32] W. Munk, P. W. and Wunsch, C., *Ocean Acoustic Tomography*. Cambridge University Press, 1995.

[33] Wapenaar, K., "Retrieving the elastodynamic greens function of an arbitrary inhomogeneous medium by cross-correlation," *Phys. Rev. Letter*, vol. 93, no. 254301, 2004.

[34] Weaver, R. L. and Lobkis, O. I., "Ultrasonics without a source: Thermal fluctuation correlations at mhz frequencies," *Physical Review Letter*, vol. 87, no. 134301, 2001.

[35] Wenz, G. M., "Acoustic ambient noise in the ocean: Spectra and sources," *J. Acoust. Soc. Am.*, vol. 34, pp. 1936–1956, 1962.